

1 **High-resolution hybrid MODIS-Landsat estimation of post-monsoon**
2 **agricultural burned area in northwestern India**

3 Tianjia Liu^{a,b}, Miriam E. Marlier^c, Alexandra N. Karambelas^d, Meha Jain^e, Sukhwinder
4 Singh^e, Manoj K. Singh^f, Ritesh Gautam^g and Ruth S. DeFries^c

5 *^aDepartment of Earth and Environmental Sciences, Columbia University, New York,*
6 *USA*

7 *^bDepartment of Earth and Planetary Sciences, Harvard University, Cambridge, USA*

8 *^cDepartment of Ecology, Evolution, and Environmental Biology, Columbia University,*
9 *New York, USA*

10 *^dThe Earth Institute, Columbia University, New York, USA*

11 *^eSchool for Environment and Sustainability, University of Michigan, Ann Arbor, USA*

12 *^fDepartment of Mathematics, University of Petroleum and Energy Studies, Dehradun,*
13 *Uttarakhand, India*

14 *^gEnvironmental Defence Fund, Washington DC, USA*

15 Corresponding author: Tianjia Liu (tianjialiu@g.harvard.edu)

16 High-resolution hybrid Landsat-MODIS estimation of post-monsoon agricultural
17 burned area in northwestern India

18 A leading source of outdoor emissions in northwestern India comes from crop
19 residue burning after the annual monsoon (*kharif*) and winter (*rabi*) crop
20 harvests. Agricultural burned area, from which agricultural fire emissions are
21 derived, is difficult to quantify due to the mismatch between moderate-resolution
22 satellite sensors and the relatively small size and short burn duration of the fires.
23 Many previous atmospheric science studies use the Global Fire Emissions
24 Database (GFED), which is based on the Moderate Resolution Imaging
25 Spectroradiometer (MODIS) burned area product MCD64A1, as a bottom-up
26 outdoor fires emissions dataset. Correction factors with MODIS active fire
27 detections have previously attempted to account for small fires. Here, we present
28 a burned area classification algorithm, complementary to MCD64A1, that
29 leverages more frequent MODIS observations (daily, 500 m) with higher spatial
30 resolution Landsat (every 16 days, 30 m) observations. Our hybrid MODIS and
31 Landsat approach is based on two-tailed, quantile-based Normalised Burn Ratio
32 (NBR) thresholds, abbreviated as ModL2T, and results in an estimated $66 \pm 31\%$
33 higher burned area than MCD64A1 in northwestern India during the 2003-2016
34 post-monsoon (October to November) burning seasons. Previous underestimation
35 of agricultural burned area suggests that the public health impacts estimates from
36 post-monsoon fires in this region are also conservative. We find moderate
37 agreement between village-level fraction of ModL2T-derived burned area and
38 surveyed farmers who burned crop residue, normalised by landholding area ($r =$
39 $0.62, p < 0.01$), in 2016. However, sources of error still arise from small median
40 landholding sizes (1-3 ha), heterogeneous spatial distribution of two dominant
41 burning practices (partial and whole field), moderate to coarse spatio-temporal
42 satellite resolution, dark soil background, cloud and haze contamination, and
43 possible conflation of burning with harvest. Our results suggest that fusion
44 methods using moderate and high resolution satellite imagery can improve
45 agricultural fire emissions inventories, thus allowing for more accurate
46 assessments of the contribution of post-monsoon agricultural fires to air quality
47 degradation and related population-weighted smoke pollution exposure in
48 northwestern India.

49 Keywords: fires; crop residue; burned area; MODIS; Landsat

50 1. Introduction

51 1.1. *Agricultural residue burning in northwestern India*

52 India is embracing agricultural mechanisation to increase crop productivity and
53 decrease labour costs in order to feed its rapidly growing population (Mehta et al.
54 2014). Agriculture in India is currently 40-45% mechanised, below that of the United
55 States, Russia, Western Europe, China and Brazil (57-95%) (Bai 2014; Mehta et al.
56 2014). India's population is expected to grow from 1.3 billion in 2015 to 1.7 billion by
57 2050 (UN 2015). This population surge demands sustainable increases in crop
58 productivity, intensity and yield, which in turn affects the rise of agricultural
59 mechanisation. Traditionally, farmers collect crop residue to feed livestock. However,
60 as India mechanises, farmers are using combine harvesters, which leave behind
61 scattered crop residues that are labour intensive to remove manually (Vadrevu et al.
62 2011; Kumar et al. 2015). Consequently, 80-90% of crop residue left behind by
63 combine harvesters is burned in field, which can severely degrade regional air quality
64 seasonally (Sidhu and Beri 2005; Government of India 2007; Singh et al. 2008; Gupta
65 2012; Liu et al. 2018). More accurate burned area estimation is a critical prerequisite for
66 improving bottom-up fire emissions inventories and quantifying public health impacts
67 from air quality degradation. In this study, we target these episodic agricultural fires and
68 build on existing methods for moderate-resolution burned area classification by
69 integrating with complementary high-resolution satellite imagery for this region.

70 In northwestern India, the timing of the double cropping system particularly
71 limits the timeframe to clear the fields of monsoon crop residue (primarily rice) during
72 the post-monsoon (October to November). Because farmers must market rice at the
73 earliest time possible and have limited time to sow the winter crop (primarily wheat),
74 they often burn the crop residue (Jain et al. 2014; PRSC 2015; Ahmed et al. 2015;
75 Gupta 2012). Thus, in spite of the restrictions on agricultural burning, farmers continue
76 to burn crop residue due to the lack of viable, well-incentivised and cost-effective
77 alternatives (Kumar et al. 2015; Ahmed et al. 2015; Gupta 2012).

78 Smoke plumes from crop residue burning blankets rural and urban areas within
79 the Indo-Gangetic Plains (IGP), which includes Punjab and Haryana, during the post-
80 monsoon (October to November) burning season (Figure 1). During pre-monsoon (April
81 to May), wheat residue is burned to prepare fields for sowing the monsoon crop. In
82 general, carbonaceous particles can be transported hundreds of kilometres in the
83 atmosphere (Sharma et al. 2010; Kaskaoutis et al. 2014). Besides air quality degradation
84 and public health impacts, crop residue burning reduces soil quality by depleting
85 organic matter, major nutrients, and microbial biomass (PRSC 2015). This inhibits the
86 productivity of the next cropping season. However, previous work using satellite fire
87 detections and HYSPLIT atmospheric back trajectories suggests that pre-monsoon
88 wheat residue burning is of less concern to the Delhi National Capital Region's air
89 quality than post-monsoon rice residue burning due to different atmospheric transport
90 patterns, higher ventilation from high boundary layer conditions, and less overall fire
91 intensity (Liu et al. 2018). While Delhi's average post-monsoon 'airshed,' or the
92 approximate region that can contribute to Delhi's air quality, encompasses most of
93 Haryana and Punjab, the average pre-monsoon Delhi airshed shifts southward, avoiding
94 high fire intensity areas. In addition, the influence of desert dust emissions and transport
95 in the post-monsoon season is minimal, in comparison to the strong dust activity during
96 pre-monsoon months (April to June), originating from the Thar desert as well as long-

97 range transport from the Arabian Peninsula. Therefore, the burned area mapping and its
98 quantification in this study is focused on the post-monsoon season.

99 [FIGURE 1]

100 **1.2. Burned area estimation of small fires**

101 The MODIS burned area product MCD64A1 (Giglio et al. 2009), on which the Global
102 Fire Emissions Database, version 4 (GFEDv4) emissions are based (Giglio et al. 2013),
103 underestimates the contribution of small fires, which has been generally accounted for
104 with a scale factor (van der Werf et al. 2010; 2017; Randerson et al. 2012; Zhu et al.
105 2017). MCD64A1 is limited by its moderate spatial resolution of 500 m x 500 m. In
106 particular, small fires < 120 ha are not well-detected (Zhu et al. 2017). Many active fires
107 in croplands are found outside the estimated burned area extent, because the
108 conservative detection threshold for burned area estimation often misses small fires
109 (Randerson et al. 2012; Zhu et al. 2017). GFEDv4s, which includes a small fires boost
110 to GFEDv4, added 79-123% in burned area to the cropland-related classes, but
111 Randerson et al. (2012) suggest that the estimate is still conservative. Thus, higher
112 spatial resolution satellite imagery is a prerequisite to more accurately estimate burned
113 area from small agricultural fires.

114 The differenced Normalised Burn Ratio (dNBR) characterises the burn extent
115 and severity of most fires over 2 km² in area on public lands (Key and Benson 2006).
116 dNBR is the difference in pre-fire and post-fire NBR. NBR is defined as:

$$117 \quad \text{NBR} = \frac{\rho_{NIR} - \rho_{SWIR}}{\rho_{NIR} + \rho_{SWIR}} \quad (1)$$

118 in which ρ_{NIR} and ρ_{SWIR} represent the surface reflectance at near infrared and
119 shortwave infrared wavelengths, respectively. Additionally, Picotte and Robertson
120 (2010) find that dNBR is suitable to map many small fires within a large landscape; this
121 is particularly relevant for agricultural fires, which are small in size and tends to cluster
122 spatially. Indeed, global and region-specific studies have used NBR-based approaches
123 to estimate small fires, including agricultural fires (e.g. Oliva and Schroeder 2015;
124 McCarty et al. 2008, 2009; Randerson et al. 2012; Zhu et al. 2017). NBR is an effective
125 indicator in mapping burn scars due to the accuracy of classification with the SWIR
126 bands (Avery and Berlin 1992; Eva and Lambin 1998) and avoidance of smoke and dust
127 susceptibility, unlike bands in the visible range of the spectrum (White et al. 1996; Roy
128 1999; Rogan and Yool 2001; Cocks et al. 2005).

129 However, burned area estimation of small agricultural fires is understudied
130 relative to that for wildfires and remains challenging for several reasons. First, the
131 drawdown in greenness attributed to fires can be conflated with harvest (Randerson et
132 al. 2012). The NBR of pre-harvest pixels are higher than post-harvest pixels, because
133 the removal of biomass during harvest decreases NBR, which is dependent on
134 vegetation greenness. Second, scene availability is limited by cloud cover and haze
135 contamination and low temporal resolution. Because pairs of pre-fire and post-fire
136 scenes are usually required, the acquisition timing of scenes is critical: NBR estimated
137 from different crop stages between pre-harvest, post-harvest, and crop residue burning
138 can affect classification. Third, unlike forest fires, which can burn continuously for days
139 over a large area, agricultural fires are relatively small, short lasting, and vary spatially
140 and temporally year-to-year based on the timing of harvest (Thumaty et al. 2015).

141 Fourth, despite severe underestimation of burned area in croplands, it is also inaccurate
142 to assume that for example, entire 500 m x 500 m MCD64A1 pixels are fully burned.
143 Thus, simple land cover type-based correction factors (Zhu et al. 2017) may be
144 insufficient without considering burn heterogeneity at higher spatial resolution.

145 Fusion MODIS-Landsat (or hybrid moderate-high resolution sensor) techniques
146 have been developed to increase the spatial resolution of burned area mapping (e.g.
147 Loboda et al. 2007; Boschetti et al. 2015). Many of these studies rely on statistical
148 methods for land change detection and/or active fire ‘hotspot’ detections as an input
149 dataset for burn scar classification. (e.g. Loboda et al. 2007; Boschetti et al. 2015; Oliva
150 and Schroeder 2015). Here, we use MCD64A1, which integrates MODIS active fires
151 into its land change detection-based burn scar algorithm (Giglio et al. 2009), as a
152 reference and training dataset for establishing NBR-based thresholds and downscaling
153 MODIS-scale burned area to Landsat resolution.

154 In this study, we develop a statistical two-tailed NBR algorithm using MODIS
155 and Landsat imagery in Google Earth Engine (Gorelick et al. 2017) to rapidly classify
156 post-monsoon (October to November) agricultural burned area in northwestern India
157 (Punjab and Haryana) from 2003-2016. The two-tailed NBR method is a two-step
158 classification based on thresholds for the pre-fire NBR_{max} and post-fire NBR_{min}
159 composites of each post-monsoon burning season. The two thresholds are derived from
160 the quantile-based intersection and separation of NBR_{min} and NBR_{max} distributions,
161 respectively, for burned and unburned agricultural areas. We compare ModL2T-derived
162 burned area (BA_{ModL2T}) to MCD64A1 and validate BA_{ModL2T} with independent
163 household survey results. In addition, we assess BA_{ModL2T} in the context of two different
164 crop residue burning practices, policy changes, mechanisation (use of combine
165 harvesters) and land fragmentation.

166 **2. Data and Methods**

167 **2.1. Study area**

168 The study area consists of two neighbouring agricultural states, Haryana (area: 44 119
169 km², 2011 population: 25.4 million) and Punjab (area: 50 427 km², 2011 population:
170 27.7 million), in northwestern India (Figure 2; <http://www.censusindia.gov.in/>).
171 Because Punjab and Haryana are situated at the heart of India’s ‘bread basket’, where
172 most farmers predominantly follow a rice (*kharif*)-wheat (*rabi*) rotation, this region is
173 an ideal area to perform high resolution analysis of burned area from small fires. For
174 our analysis, we exclude Chandigarh, an urban union territory and the capital of Punjab
175 and Haryana.

176 [FIGURE 2]

177 **2.2. Satellite data sources**

178 The datasets used in this study are primarily derived from Landsat and MODIS (Table
179 1). We primarily use Google Earth Engine (GEE) to retrieve MODIS and Landsat
180 datasets and for geospatial analysis. GEE is a cost-free, petabyte-scale cloud computing
181 platform, which has been available since 2015 (Gorelick et al. 2017). All MODIS-
182 derived products used in the burned area algorithm and assessments are from the
183 Collection 6 (C6) suite. MCD64A1 C6, which replaced MODIS C5 with C6 active fires

184 and surface reflectance products as inputs, improved on small burn scars and omission
185 errors (Giglio et al. 2016).

186 [TABLE 1]

187 *2.2.1 Double crop-fire cycle*

188 We first characterise the seasonal and diurnal temporal distributions of fires in
189 northwestern India. Following Vadrevu et al. (2011), we use the 1-km combined
190 MODIS/Terra and Aqua active fire counts (MCD14ML) to show the average annual
191 distribution of fires from 2003-2016. We also complement the fires with median NBR,
192 estimated from MODIS MOD09A1 8-day composite surface reflectance (SR) to show
193 variations in greenness in the rice-wheat double cropping system of northwestern India.
194 Giglio (2007) estimates an afternoon peak fire energy of 4.30 pm in central India based
195 on Visible and Infrared Scanner (VIRS) active fires. Central India primarily consists of
196 croplands with major *kharif* rice-growing areas (Mahajan et al. 2017). Vadrevu et al.
197 (2011) use the MODIS Terra/Aqua Fire Radiative Power (FRP) ratio to estimate a post-
198 monsoon peak fire energy of ~2.12 pm in Punjab. GFEDv4s also estimates the 3-hourly
199 diurnal cycle of fire emissions based on active fire observations from the Geostationary
200 Operational Environmental Satellite (GOES) Wildfire Automated Biomass Burning
201 Algorithm (WFABBA) (Mu et al. 2011).

202 ***2.3. The ModL2T algorithm for high-resolution burned area classification***

203 *2.3.1 Burned area estimation*

204 Previous studies on high-resolution agricultural burned area estimation in northwestern
205 India are generally constrained to 1-2 years of study (e.g. PRSC 2015; Yadav et al.,
206 2014a; 2014b). Here, we use GEE to expand the study time period to 14 years and
207 estimate post-monsoon agricultural burned area from 2003-2016. The post-monsoon
208 burning season is defined as October 1 to November 30. Figure 3 describes the
209 workflow for the ModL2T algorithm in GEE. The ModL2T algorithm can be
210 summarised as follows: (1) pre-process individual scenes; (2) composite cloud-free
211 scenes in pre-fire and post-fire collections; (3) define two-tailed thresholds based on the
212 quantile intersection of NBR in burned and unburned agricultural areas; (4) separately
213 derive MODIS and Landsat burned area; (5) merge Landsat and MODIS classifications
214 and apply agricultural mask.

215 Our method is primarily based on the MODIS MCD64A1 global burn mapping
216 algorithm and GFEDv4s small fires boost approach (Giglio et al. 2009; Randerson et al.
217 2012). We integrate moderate and high-resolution classification of seasonal fires in one
218 region and land cover type: croplands in northwestern India. MCD64A1 uses dynamic
219 NBR-based thresholds, based on 1-km MODIS active fire detections for selecting
220 burned and unburned training pixels, and is validated with Landsat-derived burned area
221 maps (Giglio et al. 2009). Here, we use MCD64A1 as a training dataset and improve on
222 MCD64A1 burned area estimation in northwestern India.

223 [FIGURE 3]

224 We use the near infrared and shortwave infrared SR bands from MODIS/Terra
225 (MOD09A1) and Landsat 5 (TM), 7 (ETM+), and 8 (OLI/TIRS) SR products to
226 estimate NBR (Table 1, S1). We use MODIS/Terra daily surface reflectance rather than
227 that of Aqua, because the local daytime overpass time of the MODIS/Terra (10.30 am)

228 – that of the MODIS/Aqua is 1.30 pm – is comparable with that of Landsat (10.00 am ±
 229 15 minutes). MOD09A1 is a gridded Level-3, validated stage 2 product that selects the
 230 best quality pixel over every 8-day period based on several criteria: cloud cover,
 231 observation coverage, low-view angle and aerosol loading (Vermote et al. 2008).

232 [TABLE 1]

233 While available MODIS/Terra and Landsat 7 scenes cover the study area for all
 234 years from 2003-2016, Landsat 5 scenes only cover 2003-2010 and Landsat 8 scenes
 235 from 2013-2016. We do not gap-fill Landsat 7 scan line errors and account for such
 236 pixels as ‘no data’. We only consider pixels as marked ‘clear’ by quality flags. Cloud-
 237 contaminated pixels are additionally filtered using the normalised difference of the
 238 SWIR and Red bands, based on Xiang et al. (2013). Visible bands are more sensitive to
 239 cloud contamination than SWIR bands; pixels where the SWIR SR exceeds Red SR are
 240 retained:

$$241 \quad \frac{\rho_{SWIR} - \rho_{Red}}{\rho_{SWIR} + \rho_{Red}} > 0 \quad (2)$$

242 Burned area from MODIS and Landsat is separately derived from NBR due to
 243 possible errors from differences in spatial resolution (500 m versus 30 m). Based on
 244 Vadrevu et al. (2011), we leverage knowledge of the timing of the *kharif* rice crop and
 245 fire activity patterns in Punjab and Haryana to define time brackets for pre-fire and
 246 post-fire image collections. MODIS and Landsat NBR_{max} (maximum NBR composite
 247 from pre-fire image collection: August 1 to September 30) and NBR_{min} (minimum NBR
 248 composite from post-fire image collection: October 1 to November 30) images serve as
 249 the two classification criteria of burned area on the basis that agricultural burned area
 250 generally have high NBR_{max} (pre-fire) and low NBR_{min} (post-fire). For croplands, the
 251 drawdown in greenness from burning can be conflated with harvest, so the drop in NBR
 252 is not as abrupt as wildfires. However, burned vegetation and ash exhibit a more
 253 negative difference between NIR and SWIR SR (or lower NBR) than bare soil (Lewis et
 254 al. 2011; Pleniou and Koutsias 2013). Thus, we expect NBR_{min} for burned fields to be
 255 lower than for unburned (fallow) fields.

256 The NBR_{max} and NBR_{min} thresholds are determined from the quantile-based
 257 separation of NBR_{max} and NBR_{min} distributions of burned and unburned agricultural
 258 areas, based on MODIS MCD64A1 burned area (500 m) and the ‘cultivated land’ class
 259 from the GlobeLand30 map for the 2010 time step (Table 1). GlobeLand30 is a global
 260 30-m, 10-class land cover map derived from > 20,000 Landsat and Chinese HJ-1
 261 satellite images (Chen et al. 2014; Chen et al. 2017; globallandcover.com). According
 262 to the University of Maryland MODIS-derived land cover classification (MCD12Q1,
 263 C5.1) from 2001-2013, cropland area does not vary significantly (standard deviation of
 264 ~1%) from year to year in the study region. We define the two-tailed classification
 265 thresholds as the average composite MODIS NBR (NBR_{min} or NBR_{max}) at the quantile-
 266 based intersection of the τ percentile of MCD64A1-burned NBR and $1 - \tau$ percentile of
 267 unburned NBR:

$$268 \quad T = \frac{1}{2} [Q_{f(X)}(\tau) + Q_{f(Y)}(1 - \tau)] \quad (3)$$

269 where T is the NBR_{max} or NBR_{min} threshold, $Q(\tau)$ is the quantile function at τ percentile
 270 of the probability density function, f , of the distribution of NBR_{min} or NBR_{max} at burned

271 (X) and unburned (Y) agricultural areas. This approach attempts to balance omission and
272 commission errors. T_{\max} ranges from 0.635 to 0.706, and T_{\min} ranges from -0.057 to -
273 0.014. The quantile-based thresholds are generally located around $\tau=0.71$ for T_{\min} and
274 $\tau=0.29$ for T_{\max} . This indicates that 71% unburned and burned agricultural areas are on
275 average separated for each threshold. We also use the MODIS-derived thresholds T_{\max}
276 and T_{\min} on Landsat NBR_{\max} and NBR_{\min} , because MCD64A1 (500 m) is relatively
277 coarse compared to Landsat resolution. Sensor-specific differences in spectral band
278 wavelengths and the lack of Landsat availability can also introduce bias (Table S1,
279 Figure S1). Thus, before deriving burned area from Landsat imagery, we correct for
280 bias in Landsat NBR composites by adding the yearly regionally-averaged differences
281 in MODIS and resampled Landsat NBR to Landsat NBR. The compensation for
282 Landsat NBR_{\max} ranges from 0.012 to 0.114, and that for NBR_{\min} ranges from -0.073 to
283 0.012. We also combine the MODIS-derived burned area with $BA_{MCD64A1}$ to minimize
284 omission error.

285 Next, to merge the separately derived MODIS and Landsat classified burned
286 area, we ‘carve’ out moderate-resolution MODIS burned pixels with high-resolution
287 Landsat burned pixels (Figure S1). That is, we are more confident in Landsat to
288 distinguish between burned and unburned fields, whereas MODIS more severely
289 homogenizes large aggregates of individual landholdings due to its coarser spatial
290 resolution. However, due to Landsat’s coarse temporal resolution, we are not confident
291 in Landsat to accurately capture the highest NBR_{\max} and lowest NBR_{\min} when its usable
292 data availability is temporally-sparse and/or biased. Thus, we first create a criterion to
293 mask such areas. After resampling to MODIS resolution, Landsat NBR_{\min} and NBR_{\max}
294 that deviate more than ± 0.1 from MODIS NBR_{\min} or NBR_{\max} are masked. With this
295 criterion, Landsat NBR_{\min} and NBR_{\max} must approximately agree with those of MODIS
296 for the ~ 238 Landsat burned and unburned pixels to take precedent and replace a
297 MODIS pixel. The NBR absolute difference threshold of 0.1 allows for some variance
298 for composites of best quality Landsat pixels from different acquisition dates and
299 sensor-specific differences in spectral band wavelengths (Table S1). While 0.1 is an
300 arbitrary selection, a large departure of Landsat from MODIS NBR indicates that pixels
301 of available Landsat scenes are generally cloudy and/or do not capture scenes near peak
302 monsoon growing season (NBR_{\max}) and/or in the post-burning (NBR_{\min}) period when
303 the burn scar is still visible. Furthermore, it may be the case that there are some Landsat
304 observations in the two-month windows for the pre-fire and post-fire collections, but the
305 acquisition dates of ‘best quality’ Landsat pixels may not be close to that for MODIS
306 pixels. In the last step, we apply an agricultural mask based on GlobeLand30 land
307 cover. The final ModL2T-derived burned area (BA_{ModL2T}) is an estimate of the total
308 post-monsoon agricultural burned area at the Landsat 30-m resolution.

309 We also assign confidence scores to BA_{ModL2T} on a pixel-by-pixel basis by
310 designating different categorical values to burned area derived from MCD64A1,
311 Landsat-only ModL2T, and MODIS (MOD09A1)-only ModL2T. We are most
312 confident in MCD64A1 and least confident in MODIS-only ModL2T, so we assign
313 $BA_{MCD64A1}$ a value of 3, Landsat-only BA_{ModL2T} a value of 2, and MODIS-only
314 BA_{ModL2T} a value of 1. Adding these burned area layers together yields a confidence
315 scale from 1 (low) to 6 (high) (Table S2).

316 2.3.2. MCD64A1-based geographical accuracy assessment

317 We use MCD64A1 as the reference dataset in a geographic accuracy assessment of the

318 two-tailed threshold burned area classification algorithm. Here, we compare MCD64A1
319 with MODIS (MOD09A1)-only BA_{ModL2T} in order to evaluate the burned area
320 classification algorithms on a pixel-by-pixel basis at the MODIS 500-m resolution. We
321 estimate Cohen's kappa coefficient (κ), which evaluates the agreement between the
322 reference and test classification after random chance is removed (Cohen 1960).

323 *2.3.3. Validation using household survey results*

324 We validate BA_{ModL2T} by using a 2016 survey on farm management practices across the
325 IGP. The 2016 survey data asks participants about burning crop residue in the post-
326 monsoon (Did you burn crop residue before planting wheat?) and includes GPS
327 coordinates. Because the survey responses inherently distinguish between burned versus
328 unburned fields, this validation addresses the conflation of burning versus harvest. We
329 use 1111 responses from farmers in 30 Punjab and 32 Haryana villages. However, the
330 GPS coordinates are located not in-field, so we cannot match responses to individual
331 fields. We therefore group responses by village name and match mean GPS coordinates
332 with an accuracy < 10 m to the village shapefiles. On average, 18 ± 5 households were
333 surveyed per village. We normalise the % households that burn crop residue with
334 landholding area by village in post-monsoon 2016. For comparison, we estimate the %
335 BA_{ModL2T} of total village cultivated area based on GlobeLand30. Due to these
336 normalised approximations spurred by data limitations, the two metrics of % burning
337 per village are not comparable in absolute terms.

338 *2.3.4. Further assessments of ModL2T-derived burned area*

339 In lieu of a single 'ground truth' validation, we further assess BA_{ModL2T} with simple
340 checks using: (1) pixel-level (active fire locations), (2) district-level (previous burned
341 area estimates) and (3) region-level (satellite aerosol optical depth, AOD). We consider
342 $p < 0.01$ to be statistically significant.

343 **Assessment 1 (VIIRS active fire locations):** The GFEDv4s small fires boost approach
344 uses the ratio of dNBR at active fire locations outside and inside burned areas
345 (Randerson et al. 2012; van der Werf et al. 2017). In line with this approach based on
346 the co-location of fires and burned area, we use higher spatial resolution (375 m)
347 Visible Infrared Imaging Radiometer Suite (VIIRS) active fire geolocations
348 (VNP14IMGML, Collection 1) over October and November in 2012-202016 to assess
349 omission errors. We consider daytime VIIRS active fire detections classified as
350 'presumed vegetation fire' (Giglio 2015). This assessment is based on the fraction of
351 VIIRS active fires co-located within the classified burned area; a higher fraction
352 indicates a lower omission error. BA_{ModL2T} is first resampled to 375 m to approximately
353 match VIIRS spatial resolution to account for uncertainty in VIIRS active fire
354 geolocations.

355 **Assessment 2 (previous burned area estimates):** We compare post-monsoon district-
356 level BA_{ModL2T} to that of PRSC (2015) and Yadav et al. (2014a; 2014b). PRSC (2015)
357 estimated district-level burned area from post-monsoon burning in Punjab in 2014 and
358 2015 by performing classification on multi-date Normalised Difference Vegetation
359 Index (NDVI) from high-resolution multi-sensor (Landsat 8, AWiFS and LISS-3)
360 satellite imagery from October 15 to November 15. Yadav et al. (2014a; 2014b) used
361 the Iterative Self-Organising Data Analysis (ISODATA) clustering classifier in multi-
362 date unsupervised classification of AWiFS satellite-derived NDVI images to estimate

363 agricultural burned area in ten districts (Ambala, Faridabad, Jind, Kaithal, Karnal,
364 Kurukshetra, Panipat, Sirsa, Sonapat and Yamunanagar) in northern Haryana in 2013
365 and three districts (Kaithal, Karnal and Kurukshetra) in 2010, respectively. PRSC
366 (2015) and Yadav et al. (2014a; 2014b) validated district-level burned area
367 classifications using ground truth GPS points and/or field photographs.

368 **Assessment 3 (MODIS AOD):** Aerosol optical depth (AOD) represents the column-
369 integrated aerosol loading and measures the extinction of solar radiation. High AOD
370 values represent hazy conditions and generally poor air quality. We use Level-2 AOD
371 product from MODIS/Terra, operationally available at 3 km and 10 km pixel resolution,
372 to assess detrended correlation with BA_{ModL2T} (Table 1). Mid-visible AOD retrievals at
373 $0.55 \mu\text{m}$ are used in this study. The Level-2 AOD retrievals are available on a daily
374 basis, which were then uniformly gridded to produce a per-pixel AOD mean spatial
375 distribution at $3 \times 3 \text{ km}$ and $10 \times 10 \text{ km}$ grid cells, for Punjab and Haryana. The data
376 were then averaged for each post-monsoon period from 2003-2016. For the 10 km AOD
377 retrieval, we use the combined Dark-Target (DT) and Deep-Blue (DB) product, which
378 merges aerosol retrievals over both dark vegetated and bright reflecting regions (e.g.
379 arid/desert areas except snow surface) (Singh et al. 2017). In terms of accuracy of the 10
380 km product, the expected error envelope is reported to be $\pm(0.05 + 0.15\tau)$ over land
381 (Levy et al. 2013) for DT retrievals and $\pm(0.03 + 0.2\tau)$ for DB retrievals (Sayer et al.
382 2013), where τ represents AOD. This combined DT/DB product uses NDVI climatology
383 for differentiating between dark and bright land areas. In this study, we use the best-
384 quality retrievals of the combined DT/DB AOD data (for only quality flag = 3
385 retrievals). Additionally, the 3 km AOD retrievals are also used to analyse spatial
386 distribution of aerosol loading at a higher resolution and study relationship with burned
387 area. The 3 km AOD data are based on DT retrievals, limited to vegetated pixels, which
388 cover the majority of Punjab and Haryana. The uncertainty of the 3 km AOD retrieval is
389 reported as $\pm(0.05 + 0.15\tau)$ (Munchak et al. 2013), where τ represents AOD.

390 **2.4 Landholdings and combine harvesters**

391 We consider ancillary data in landholding size and combine harvester use to assess
392 trends in farm fragmentation and mechanisation. The Agricultural Census division of
393 Indian Department of Agriculture, Cooperation, and Farmers Welfare conducts the
394 Agricultural Census in India (<http://agcensus.nic.in/>) and provides two online databases:
395 Agricultural Census and Input Survey. The online database of the Agricultural Census,
396 which is based on census and input sample survey, contains quinquennial data regarding
397 the number, average size and area of landholdings by country, state, district and tehsil
398 (sub-district) and by social group (caste, tribe) and gender from 1995-96 to 2010-11
399 (<http://agcensus.dacnet.nic.in/>). The Input Survey is another online database with
400 quinquennial data of detailed information about agricultural implements and machinery,
401 including total combine harvesters by landholding size, from 1996-97 to 2011-12
402 (<http://inputsurvey.dacnet.nic.in/>). The 2016 household survey also asks participants
403 about harvest methods (How do you harvest your rice crop?). The possible response
404 choices are: (1) fully mechanical (e.g. combine harvester), (2) partially mechanical (e.g.
405 thresher), (3) manually, (4) both manual and mechanical, (5) other and (6) never
406 harvested rice. We use all responses from farmers in Punjab and Haryana to assess the
407 relationship between combine harvester use and rice residue burning before sowing
408 wheat.

409 **2.5. Methods of crop residue burning**

410 In a field visit, Kumar et al. (2015) identified two dominant crop residue burning
411 practices in Punjab: (1) whole field burning and (2) partial burning (small stalks). We
412 use Google Earth's collection of fine-resolution imagery (DigitalGlobe and CNES/
413 Airbus) to qualitatively characterise crop residue burning practices (e.g. whole field,
414 partial field burning) at the resolution of individual fields in Punjab and Haryana. We
415 discuss the differences in scarring from and spatial distribution of the two dominant
416 burning practices. Most scenes assessed were acquired in 2014-2016.

417 **3. Results**

418 **3.1. Spatio-temporal distributions in fire activity**

419 Figure 4(a) shows the average annual timing of the bimodal fire activity and the double-
420 crop system in northwestern India. Whereas high NBR represents high vegetation cover
421 (peak greenness) during the monsoon and winter crop growing seasons, low NBR
422 represents low vegetation cover (bare soil, burn scars) after harvest and crop residue
423 burning. MCD64A1 burn frequency shows repeated post-monsoon fire activity from
424 2003-2016, particularly in southern-central Punjab (Figure 4(b)), where fires tend to
425 occur later in the fire season than in parts of northern Punjab (Figure 4(c)). In addition,
426 Aqua (1.30 pm local time) averages 645 ± 289 % higher in fire counts than Terra (10.30
427 am local time) during the 2003-2016 post-monsoon burning seasons, which is consistent
428 with the afternoon peak fire energy (4.30 pm local time) estimated by Giglio (2007).
429 Estimates from 3-hourly GFEDv4s, based on Mu et al. (2011), and Vadrevu et al.
430 (2011) point to an earlier (~ 2.12 pm local time) post-monsoon peak fire energy in
431 Punjab (Figure S3). However, Vadrevu et al. (2011) is limited by MODIS Terra/Aqua
432 overpass times, and Mu et al. (2011) use land cover type matching to broadly attribute
433 normalized fire diurnal cycles globally based on GEOS observations in North and South
434 America.

435 [FIGURE 4]

436 **3.2. ModL2T-derived burned area**

437 **3.2.1. Comparison to MCD64A1 burned area estimates**

438 The strength of agreement (Cohen's κ) between $BA_{MCD64A1}$ and MODIS-only BA_{ModL2T}
439 is consistent and ranges from 0.4-0.53 (moderate) (Landis and Koch 1977). Overall
440 accuracy ranges from 82-89%. ModL2T averages 66 ± 31 % higher post-monsoon
441 burned area than MCD64A1 in Punjab and Haryana from 2003-2016 (Figure 5).
442 BA_{ModL2T} in 2003-07 and 2011-12 may be less accurate as a result of relatively low
443 availability of usable and cloud-free data for MODIS and/or Landsat (Figures S1, S2).
444 Proportionally, $BA_{MCD64A1}$ in Haryana constitutes a smaller fraction (14 ± 3 %) of total
445 burned area in the study region than BA_{ModL2T} (24 ± 3 %). This indicates that the
446 ModL2T increase in burned area over MCD64A1 is partly driven by its additional burn
447 scar detections in Haryana.

448 [FIGURE 5]

449 3.2.2. Validation with 2016 household survey

450 Figure 6(a) shows the spatial comparison between $BA_{MCD64A1}$ and MODIS-only
451 BA_{ModL2T} in 2016. The overall accuracy is 84% with moderate agreement ($\kappa = 0.53$)
452 (Table 2). Disagreements between $BA_{MCD64A1}$ and MODIS-only BA_{ModL2T} mainly lie in
453 central Haryana and northern Punjab.

454 [FIGURE 6]

455 [TABLE 2]

456 We validate BA_{ModL2T} with independent household survey results from 2016.
457 We compare post-monsoon village-level survey crop residue burning rates, normalised
458 by landholding size, with BA_{ModL2T} expressed as a fraction of cropland area. The
459 village-level fraction of surveyed households that burn crop residue is moderately
460 correlated with fractional BA_{ModL2T} ($r = 0.62, p < 0.01$) (Figure 7(a)). In contrast,
461 $BA_{MCD64A1}$ achieves a weaker correlation of $r = 0.54$ ($p < 0.01$) and tends to cluster at
462 fractions burned of 0 or 1, likely due to its moderate spatial resolution (Figure 7(b)).
463 $BA_{MCD64A1}$ and BA_{ModL2T} explain 28% and 37% of variability in survey burn rates,
464 respectively, indicating that BA_{ModL2T} is better able to capture variability in the ‘ground
465 truth’ burn rates.

466 [FIGURE 7]

467 3.2.3. Additional assessments of BA_{ModL2T} and $BA_{MCD64A1}$

468 We first assess omission error based on the fraction of VIIRS active fire detections co-
469 located with $BA_{MCD64A1}$ and BA_{ModL2T} , during the 2012-2016 post-monsoon burning
470 seasons. With a higher spatial resolution (375 m) than MODIS/Terra and Aqua (1 km),
471 VIIRS is able to more consistently detect smaller and cooler fires (Figure S4). We find
472 that BA_{ModL2T} , resampled to 375 m, and $BA_{MCD64A1}$ are co-located with 92-99% (1-8%
473 omission error) and 45-59% (41-55% omission error), respectively, of VIIRS-detected
474 active fires within cropland areas (Table S3). In particular, $BA_{MCD64A1}$ is unable to
475 detect small burn scars in central Haryana (Figures 6, S4). Over the 5-year period from
476 2012-2016, VIIRS detected active fires in 55% of the grid cells in Punjab and Haryana,
477 while MODIS only detected active fires in 39% of the area (Figure S4c). In addition,
478 VIIRS detected that 15% of grid cells burned consecutively during post-monsoon from
479 2012-2016, while MODIS only detected 1% of grid cells by this criterion.

480 Next, we compare district-level burned area from previous estimates (PRSC
481 2015; Yadav et al. 2014a; 2014b) to BA_{ModL2T} . Total Punjab BA_{ModL2T} is 5% lower and
482 18% higher than that of PRSC (2015) in 2014 and 2015, respectively. In contrast,
483 Punjab $BA_{MCD64A1}$ is lower than PRSC (2015) burned area estimates in both 2014 and
484 2015 by 20% and 3%, respectively (Figure S5). However, for northern Haryana
485 districts, ModL2T and MCD64A1 both tend to overestimate burned area relative to
486 Yadav et al. (2014a; 2014b). District-level BA_{ModL2T} ($r = 0.88, p < 0.01$) and $BA_{MCD64A1}$
487 ($r = 0.87, p < 0.01$) are strongly correlated with PRSC (2015 and Yadav et al. (2014a;
488 2014b) burned area estimates. In terms of mean absolute error, ModL2T (257 km²)
489 outperforms MCD64A1 (279 km²).

490 Finally, we assess 14-year trends and detrended interannual variations in mean
491 MODIS AOD and BA_{ModL2T} . We find increased aerosol loading in ground-based
492 column AOD measurements, during October-November, from the Aerosol Robotic
493 Network (AERONET) site at Lahore (in the neighbouring Pakistan province of Punjab)

494 (Figure S6). Previous work of using HYSPLIT trajectories with MODIS FRP suggests
495 that AOD weakly and positively co-varies with fire intensity during post-monsoon (Liu
496 et al. 2018). Due to potential long-range atmospheric transport of aerosols from the fire
497 source region, we consider trends and interannual variability at coarse spatial scale. In
498 the 14-year time span, satellite AOD increased by $0.017 \pm 0.003 \text{ yr}^{-1}$ ($p < 0.01$) and
499 $\text{BA}_{\text{ModL2T}}$ by $713 \pm 115 \text{ km}^2 \text{ yr}^{-1}$ ($p < 0.01$) (Figure S7a-b). While not statistically
500 significant at the 99% significance level, regional $\text{BA}_{\text{ModL2T}}$ is weakly positively
501 correlated with mean regional AOD for both the 3 km ($r = 0.39$, $p = 0.17$) and 10 km (r
502 $= 0.36$, $p = 0.21$) datasets (Figure S6c). Comparatively, $\text{BA}_{\text{MCD64A1}}$ is anti-correlated
503 with mean regional AOD (3 km AOD: $r = -0.43$, $p = 0.13$; 10 km AOD: $r = -0.54$, $p <$
504 0.05) (Figure S7d).

505 **3.3. Trends in landholding size and combine harvesters**

506 The median landholding size in Haryana (1-2 ha) is smaller than that of Punjab (2-3 ha);
507 only ~0.5% of landholdings in Haryana and ~1% in Punjab are over 20 ha (Figure 8).
508 After some consolidation of small landholdings from 1995-96 to 2000-01, landholdings
509 were increasingly fragmented from 2000-01 to 2010-11. Landholdings smaller than 7.5
510 ha increased from 88.2% to 89.5% of total landholdings in Haryana and 75.4% to
511 77.1% in Punjab from 2000-01 to 2010-11. Simultaneously, the number of combine
512 harvesters tabulated by the Indian Input Survey increased 20-fold from 14 664 in 1996-
513 97 to 297 132 in 2011-12 in Haryana and almost 3-fold from 93 191 in 1996-97 to 256
514 162 in 2011-12 in Punjab. In the 2016 household survey, 68% of surveyed farmers that
515 used a combine harvester to harvest rice subsequently burned the crop residue in
516 preparation for sowing wheat in Punjab and Haryana. Of those who burned crop
517 residue, 93% used fully or partially mechanical methods of harvesting.

518 [FIGURE 8]

519 **3.4. Two burning practices: size and shape of burn scars**

520 Based on fine-resolution DigitalGlobe and CNES/ Airbus historical imagery in
521 November 2016, we observe two dominant crop residue burning practices in the study
522 region that Kumar et al. (2015) observed in a field visit in Punjab: burning of (1) whole
523 fields and (2) piled-up loose residue at the centre of fields (Figure 9). Although farmers
524 in Punjab and Haryana seem to employ a mixture of the two burning practices, available
525 DigitalGlobe and CNES/ Airbus images of the study region suggest that farmers in
526 Punjab tend to fully burn fields and some Haryana farmers partially burn fields post-
527 harvest. Kumar et al. (2015) also concluded that whole-field burning is more popular in
528 practice than partial burning in Punjab. Whole-field burning induces dark scarring of
529 entire fields such that adjoining fields burned in this way within days of each other are
530 starkly contrasted against the surrounding unburned landscape (Figure 9(a-b)). In
531 contrast, partial burning leaves circular or ring-shaped scarring in the centre of fields;
532 only ~1/9 of the field area is in fact scarred (Figure 9(c-d)).

533 [FIGURE 9]

534 4. Discussion

535 4.1. ModL2T-derived burned area: validation, assessments, and uncertainties

536 In this study, we use MODIS and Landsat imagery to estimate post-monsoon
537 agricultural burned area in northwestern India for 14 years from 2003-2016. Use of
538 Landsat imagery has been primarily limited by: (1) its low temporal resolution (16 days)
539 and (2) storage and computing power. To minimize these limitations, we implement a
540 hybrid MODIS-Landsat approach in Google Earth Engine, a cloud-computing platform
541 with petabyte-scale storage, to rapidly process large collections of MODIS and Landsat
542 imagery and expand the spatio-temporal range of study.

543 In comparison to MCD64A1, the ModL2T algorithm estimates on average $66 \pm$
544 31% higher burned area in Haryana and Punjab during post-monsoon, from 2003-2016.
545 We validate the BA_{ModL2T} with survey data from 2016. The higher correlation ($r = 0.62$,
546 $p < 0.01$) between village-level fractions of households that burn crop residue,
547 normalised by landholding area, and BA_{ModL2T} , compared to $BA_{MCD64A1}$ ($r = 0.54$, $p <$
548 0.01), of total village cropland area suggests that the ModL2T algorithm can estimate
549 burned area with increased accuracy. According to this validation, both ModL2T and
550 MCD64A1 tend to underestimate burned area in northern Punjab villages and
551 overestimate that in northeastern Haryana villages. The homogenous definition of the
552 time range for pre-fire and post-fire collections for the ModL2T algorithm may have
553 restricted burned scar detection. For example, the northern Punjab districts of
554 Kapurthala and Jalandhar tend to burn earlier than other districts. Thus, more spatially
555 dynamic temporal specifications of the pre-fire and post-fire image collections and
556 detailed knowledge of the cropping patterns may decrease omission errors.

557 In additional assessments, we find that BA_{ModL2T} improves on $BA_{MCD64A1}$ in
558 terms of omission error, comparison with previous estimates of burned area, and
559 relationship with satellite AOD. First, we find that BA_{ModL2T} captures 92-99% of VIIRS
560 active fires within its extent, while $BA_{MCD64A1}$ is only co-located with 45-59% of VIIRS
561 active fires. Second, BA_{ModL2T} improves on $BA_{MCD64A1}$ in terms of mean absolute error
562 relative to previous district-level burned area estimates (PRSC 2015; Yadav et al.
563 2014a; 2014b). The strong overall agreement ($r = 0.87-0.88$, $p < 0.01$) with PRSC
564 (2015) and Yadav et al. (2014a; 2014b) burned area suggests that the ModL2T and
565 MCD64A1 can achieve burned area estimates similar to methods using high-resolution
566 satellite imagery, supervised classification, and ground truth validation at the district-
567 level. Finally, we find commensurate increasing trends in burned area and satellite AOD
568 from 2003-2016, suggesting increasing fire activity and hazier conditions over the
569 region. In addition, we find that BA_{ModL2T} exhibits a weak positive correlation with
570 satellite AOD, after detrending, but still improves on the anti-correlation observed with
571 $BA_{MCD64A1}$.

572 Of course, these validation and assessments are also subject to various
573 limitations and uncertainties. For example, the 2016 household survey is spatially
574 constrained to northeastern Haryana and northern Punjab and may be not representative
575 of entire villages, as some villages have a small sample size. Without in-field GPS data
576 and more detailed information on burn practices, we did not take into account partial
577 burning and assumed a field is entirely burned if a farmer affirms crop residue burning.
578 Similar to MODIS, VIIRS active fires are limited by overpass times and the short burn
579 duration of agricultural fires. Further, by only using satellite imagery with high spatial

580 resolution but low temporal resolution, PRSC (2015) and Yadav et al. (2014a; 2014b)
581 burned area estimations are more susceptible to cloud and haze contamination and
582 limited usable scenes. Finally, satellite AOD can be influenced by other local and
583 regional post-monsoon pollution sources, such as dust, coal combustion, and Diwali
584 festival fireworks (Cusworth et al. 2018). While the % valid pixels used for estimating
585 mean regional AOD is relatively consistent across years ($38 \pm 3\%$), Cusworth et al.
586 (2018) found that active fires under thick haze are underdetected, thereby masking
587 critical AOD measurements for days with severe haze.

588 ***4.2. Limitations of burned area algorithms in northwestern India***

589 $BA_{MCD64A1}$, which the GFEDv4s fire emissions inventory relies on, is derived from
590 MODIS, a moderate-resolution satellite (500 m). In India, however, the average
591 landholding tends to be comparatively small and fragmented (Misri 1999). In Punjab
592 and Haryana, only 0.5-1% of landholdings are > 20 ha, comprising just 7-8.6% of total
593 area. Because prescribed agricultural burning is constrained by landholding size, the
594 estimation of small fires burned area is important in Punjab and Haryana. The
595 Randerson et al. (2012) and van der Werf et al. (2017) approach for estimating the small
596 fires contribution in GFEDv4s relies on two ratios: (1) FC_{out}/FC_{in} , or the ratio of active
597 fires outside to those inside the $BA_{MCD64A1}$ extent for each $0.25^\circ \times 0.25^\circ$ grid cell and
598 (2) $(dNBR_{out} - dNBR_{control}) / (dNBR_{in} - dNBR_{control})$, or the ratio that represents the dNBR
599 outside and inside $BA_{MCD64A1}$ relative to an unburned control area. This methodology
600 assumes confidence in $BA_{MCD64A1}$ to be from more spatially expansive fires and a linear
601 correlation of burn severity with burned area (Randerson et al. 2012). However, unlike
602 wildfires, whose burn severity and burned area extent can vary greatly, cropland fires
603 are usually controlled in burn rate, time and area, thus limiting the upper bound of burn
604 severity and burned area extent per fire. For cropland fires, dNBR has been used more
605 as a threshold for burned area classification than a proxy for burn severity (e.g. McCarty
606 et al. 2008; 2009; Oliva and Schroeder 2015; Zhu et al. 2017). Furthermore, in
607 northwestern India, the time pressures of the double-crop system forces a quick harvest-
608 to-sowing turnaround time during post-monsoon (Kumar et al. 2015). The 16-day
609 composite MOD13A1 SR product may be too temporally coarse for cropland dNBR in
610 that it collects the best quality pixels and could miss the lowest NBR pixels immediately
611 post-fire.

612 Moreover, based on the two dominant types of burning practices (whole and
613 partial field burning) as seen in DigitalGlobe images of Punjab and Haryana during the
614 post-monsoon burning season, the method in which farmers pile up loose crop residue
615 in the centre of the field for burning (particularly in Haryana) may be more difficult to
616 detect due to sub-landholding size fires. Of course, this difficulty is compounded by
617 small median landholding sizes in Haryana (1-2 ha) and Punjab (2-3 ha). Particularly in
618 Haryana, the potential prevalence of partial burning, in conjunction with small median
619 landholding size (1-2 ha), makes it more difficult for moderate-resolution satellites to
620 detect agricultural fires and accurately estimate burned area. The pile-up residue method
621 only burns the centre of fields ($\sim 1/9$ of field area), leaving a centred ring-shaped mark,
622 while whole field burning blackens the entire field. Thus, if a GFED grid cell contains a
623 small sample of large or small fires, the dNBR ratio used in the small fire boost
624 algorithm may be inaccurate. Similarly, if no or little $BA_{MCD64A1}$ is present within a grid
625 cell, the potential of the small fires boost is limited. These challenges, some region-
626 specific, are reflected in the performance of the GFEDv4s small fires boost (Randerson
627 et al. 2012; van der Werf et al. 2017): added small fires emissions from 2003-2016

628 average ~20% of total post-monsoon Punjab and Haryana emissions, compared to ~47%
629 of annual global agricultural emissions.

630 Finally, GFEDv4s and MCD64A1, both of which use active fire detections, are
631 by extension susceptible to spatio-temporal limitations in MODIS satellite overpass
632 times and detection limit. In India, agricultural fires typically last no more than half an
633 hour (Thumaty et al. 2015). VIIRS, at a higher resolution (375 m), detected 44% more
634 0.01° x 0.01° grid cells with active fires than MODIS/Terra and Aqua from 2012-2016.
635 Even so, VIIRS would not be able to detect small and cool fires and fires below optically
636 hazy areas and outside of its overpass time. For example, if the peak fire energy is close
637 to the late afternoon time (4.30 pm local time) estimated by Giglio (2007), the earlier
638 daytime overpass times of MODIS/Terra and Aqua (10.30 am and 1.30 pm,
639 respectively) and VIIRS (1.30 pm) imply missed fire detections. Oliva and Schroeder
640 (2015) show that VIIRS-derived burned area compares poorly to a Landsat 8 reference
641 dataset; in north India, the VIIRS fire detection rate was only 7.75% for fires < 10 ha
642 and 28.82% for those > 10 ha.

643 Due to the short time window to detect burn scars and region-specific
644 limitations, namely landholding size and variations in burning practices, sub-weekly,
645 sub-Landsat resolution imagery is required to fine-tune burned area estimates at the
646 landholding level. The low temporal availability of Landsat increases its susceptibility
647 to low pixel availability from haze and clouds. Several scenes cover the study region,
648 and the mismatch in date acquired may cause incongruity if one scene is hazy and
649 cloudy. Further, although we use MOD09A1 (8-day composite) as the surface
650 reflectance product instead of MOD13A1 (16-day composite) used in Randerson et al.
651 (2012) and van der Werf et al. (2017), MOD09A1 may still be too coarse in temporal
652 resolution. Thus, the limited overpass frequency of available satellite imagery from
653 MODIS and Landsat suggests that the burned area estimates in this study are still likely
654 conservative.

655 ***4.3. Implications of groundwater policy, increasing mechanisation and land*** 656 ***fragmentation***

657 In 2009, the Punjab and Haryana governments implemented the “Preservation of Sub-
658 soil Water Act, 2009” (Ordinance in 2008) to counteract groundwater depletion by
659 delaying rice transplanting to after June 10 and 15, respectively. In effect, this policy
660 forces the rice harvest season to extend to mid-November (Bhullar and Bhullar 2013;
661 Singh 2009; PRSC 2015). Based on the 2016 household survey, 76% of farmers in
662 Punjab and Haryana ideally prefer to sow wheat before November 15, but only 44%
663 were able to sow wheat before mid-November. This ideal-actual sow date difference is
664 starker for farmers who burned crop residue: 78% prefer to sow before mid-November,
665 and only 35% sowed before this date. We find a step increase of ~28% in average
666 BA_{ModL2T} from the 2003-07 to 2008-16 time period. A two-sample t-test shows that the
667 difference in BA_{ModL2T} between the two time periods is statistically significant ($p <$
668 0.01) with a difference of 5762 km² (95% CI: [3086, 8438] km²). However, further
669 work is needed to robustly quantify the effect of potential delays in rice harvests and
670 agricultural fires on a finer temporal scale, or daily to weekly basis.

671 In northwestern India, agricultural mechanisation, combined with the time-
672 intensive double-crop system, drives crop residue burning. Combine harvesters,
673 normalised by total landholdings, increased by 58% from 2001-02 to 2011-12.
674 However, at the same time, % landholdings < 7.5 ha increased by ~1.5% from 2000-01

675 to 2010-11 in Punjab and Haryana. Increasing land fragmentation may slow the rate of
676 agricultural mechanisation as marginal and small landholdings become too fragmented
677 to be mechanised or mechanised in the same way as medium and large landholdings
678 (Deininger et al. 2017; Mehta et al. 2014). Specifically, the widening technology gap
679 between marginal to small (manual and animal-drawn) and medium to large (tractor-
680 drawn and self-propelled) landholdings may be reduced through consolidation (Mehta
681 et al. 2014). However, if consolidation efforts strengthen as a result of the demand for
682 higher crop productivity and agricultural mechanisation, crop residue burning rates may
683 accelerate unless alternative, more sustainable methods become viable and cost-time
684 effective.

685 ***4.4. Future directions for burned area mapping and fire emissions inventories***

686 The recent proliferation of finer resolution satellites, such as VIIRS (375 m, daily, post-
687 2012), Sentinel-2 (10-20 m, every 5 days, post-2015) and Planet (<5 m, daily, post-
688 2016), offers added potential for active fire and burn scar detection (Drusch et al. 2012;
689 Strauss 2017). Integration of these products with the hybrid MODIS-Landsat framework
690 can improve accuracy in burned area estimation and fire emissions inventories for more
691 recent years of study (e.g. Wang et al. 2017). For example, the emissions factor for
692 partial burning may be higher than whole field burning, but its burn scar is sub-
693 landholding size and its emissions footprint is therefore difficult to estimate even at
694 Landsat resolution. Fine resolution sensors can be used to distinguish the spatial
695 patterns of the burning practices to better inform fire emissions inventories retroactively
696 and proactively. Additionally, the coupling of cloud computing and geospatial datasets
697 in GEE makes near-real time analysis possible for policy and management decisions
698 (Gorelick et al. 2017). Rapid availability of updated collections of satellite-derived
699 products on GEE can decrease the turnover time for new versions of fire emissions
700 inventories, such as GFEDv4s, which currently uses MCD64A1 C5.1 (van der Werf et
701 al. 2017). Finally, due to high uncertainties associated with small cropland fires, we
702 recommend that global burned area and fire emissions datasets use ground truth data in
703 northwestern India to train and validate algorithms.

704 **5. Conclusion**

705 The two-fold problem of satellite spatial and temporal limitations poses a difficult
706 challenge for estimating burned area from agricultural fires. In particular, the small
707 landholdings in the region and the short duration of agricultural fires require both high
708 spatial and temporal satellite resolution. MODIS burned area product MCD64A1 is
709 limited by moderate spatial resolution (500 m), and the GFEDv4s small fires boost to
710 MCD64A1 further limits the spatial resolution (0.25°). In this study, we develop a
711 hybrid approach (ModL2T) that leverages the temporal resolution of MODIS (daily,
712 500 m) and spatial resolution of Landsat (every 16 days, 30 m) in a two-step NBR-
713 based classification. Additionally, we use the Google Earth Engine platform to rapidly
714 run the ModL2T algorithm using all available MODIS and Landsat images within the
715 defined pre-fire and post-fire time periods to classify post-monsoon (October to
716 November) burned area. The ModL2T algorithm estimates $66 \pm 31\%$ higher post-
717 monsoon burned area than MCD64A1 in Punjab and Haryana from 2003-2016. In
718 future work, the high-resolution BA_{ModL2T} (30 m) dataset, which moderately well agrees
719 ($r = 0.62$) with independent household survey results, can be used to build an emissions

720 inventory for post-monsoon agricultural fires in Punjab and Haryana and re-evaluate –
721 and likely previously underestimated – regional public health effects. Lastly, the
722 methods described in this study may be useful in other regions with high concentrations
723 of small fires and in improving global fire emissions inventories currently based on
724 moderate-resolution satellite products.

725 **Acknowledgements**

726 We acknowledge the Columbia University Department of Earth and Environmental
727 Sciences Young Investigator Award and Earth Institute Research Assistantship program
728 for support for this work, as well as the Columbia University President’s Global
729 Innovation Fund. This work was also supported by a National Science Foundation
730 Graduate Research Fellowship awarded to T.L. (Award Number DGE1144152 and
731 DGE1745303). The household survey in 2016 was funded by a NSF SEES Postdoctoral
732 Fellowship (Award Number 1415436) to M.J. We also thank Dr Brent Holben for
733 establishing and maintaining AERONET Lahore, Pakistan site.
734

735 **References**

- 736 Ahmed, T., B. Ahmad, and W. Ahmad. 2015. “Why do farmers burn rice residue?
737 Examining farmers’ choices in Punjab, Pakistan.” *Land Use Policy* 47: 448-458.
738 doi:10.1016/j.landusepol.2015.05.004.
- 739 Avery, T. E. and G. L. Berlin. 1992. *Fundamentals of remote sensing and airphoto*
740 *interpretation*. Upper Saddle River: Prentice Hall.
- 741 Bai, R. 2014. “Analysis of the Trends of Agricultural Mechanisation Development in
742 China (2000-2020).” *ESCAP/CSAM Policy Brief*, Issue No.1. [http://www.un-](http://www.un-csam.org/publication/PB201401.pdf)
743 [csam.org/publication/PB201401.pdf](http://www.un-csam.org/publication/PB201401.pdf).
- 744 Bhullar, G. S. and N. K. Bhullar. 2013. *Agricultural Sustainability: Progress and*
745 *Prospects in Crop Research*. London: Academic Press/Elsevier.
- 746 Boschetti, L., D. P. Roy, C. O. Justice, and M. L. Humber. 2015. “MODIS–Landsat
747 fusion for large area 30 m burned area mapping.” *Remote Sensing of*
748 *Environment*. 161: 27-42. doi:10.1016/j.rse.2015.01.022.
- 749 Chen, J., Ban, Y., and Li, S. “Open access to Earth land-cover map.” *Nature*. 514: 434.
750 doi:10.1038/514434c.
- 751 Chen, J., Cao, X., Peng, S., and Ren, H. 2017. “Analysis and Applications of
752 GlobeLand30: A Review.” *International Journal of Geo-Information*. 6: 230.
753 doi:10.3390/ijgi6080230.
- 754 Cocke, A. E., P. Z. Fulé, and J. E. Crouse. 2005. “Comparison of burn severity
755 assessments using Differenced Normalised Burn Ratio and ground data.”
756 *International Journal of Wildland Fire* 14(2): 189-198. doi:10.1071/WF04010.
- 757 Cohen, J. 1960. “A coefficient of agreement for nominal scales.” *Education and*
758 *Psychological Measurement* 20(1): 37-46. doi:10.1177/001316446002000104.
- 759 Cusworth, D. H., L. J. Mickley, M. P. Sulprizio, T. Liu, M. E. Marlier, R. S. DeFries, S.
760 K. Guttikunda, and P. Gupta. 2018. “Quantifying the influence of agricultural

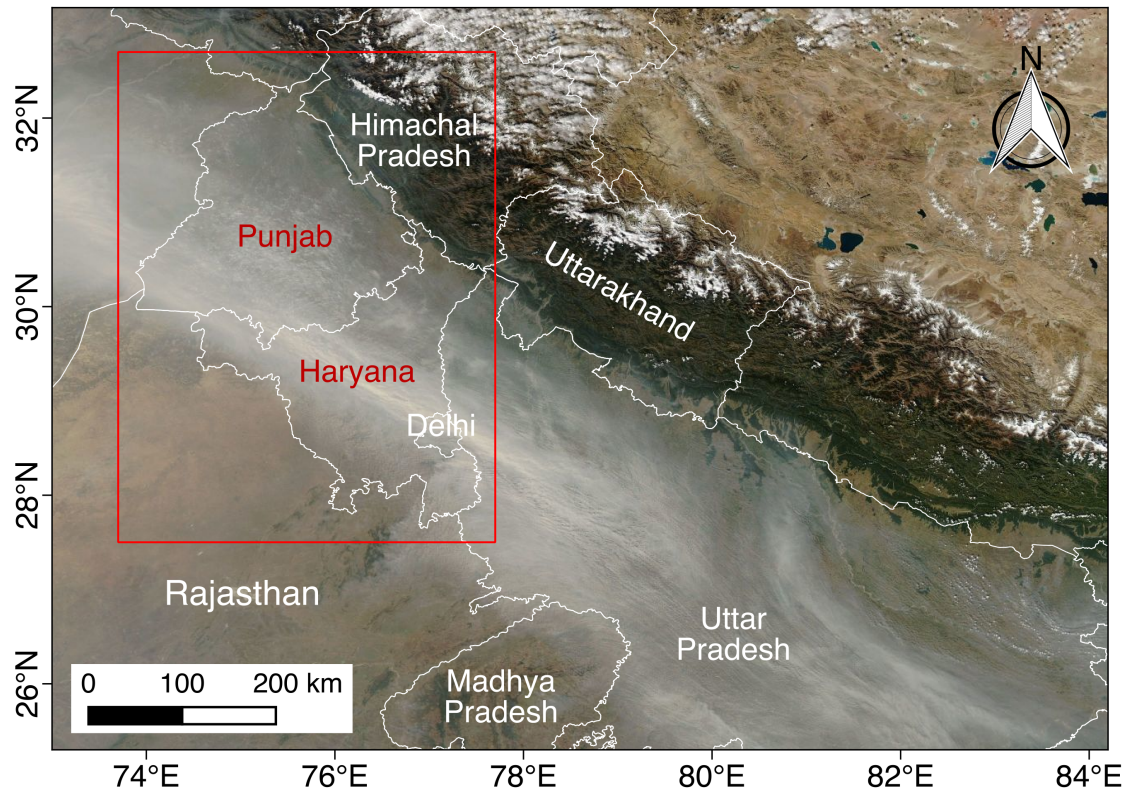
- 761 fires in northwest India on urban air pollution in Delhi, India.” *Environmental*
762 *Research Letters*. In Press.
- 763 Deininger, K., D. Monchuk, H. K. Nagarajan, and S. K. Singh. 2017. “Does Land
764 Fragmentation Increase the Cost of Cultivation? Evidence from India.” *The*
765 *Journal of Development Studies* 53(1): 82-98. doi:
766 10.1080/00220388.2016.1166210.
- 767 Drusch, M., U. Del Bello, S. Carlier, O. Colin, V. Fernandez, F. Gascon, B. Hoersch, C.
768 Isola, P. Laberinti, P. Martimort, A. Meygret, F. Spoto, O. Sy, F. Marchese, and
769 P. Bargellini. 2012. “Sentinel-2: ESA’s optical high-resolution mission for
770 GMES operational services.” *Remote Sensing of Environment* 120: 25–36. doi:
771 10.1016/j.rse.2011.11.026
- 772 Eva, H. and E. F. Lambin. 1998. “Burnt area mapping in Central Africa using ATSR
773 data.” *International Journal of Remote Sensing* 19(18): 3473-3497.
774 doi:10.1080/014311698213768.
- 775 Giglio, L. 2007. “Characterisation of the tropical diurnal fire cycle using VIRS and
776 MODIS observations.” *Remote Sensing of Environment* 108(4): 407-421.
777 doi:10.1016/j.rse.2006.11.018.
- 778 Giglio, L., T. Loboda, D. P. Roy, B. Quayle, and C. O. Justice. 2009. “An active-fire
779 based burned area mapping algorithm for the MODIS sensor.” *Remote Sensing*
780 *of Environment* 113(2): 408-420. doi:10.1016/j.rse.2008.10.006.
- 781 Giglio, L., J. T. Randerson, and G. R. van der Werf. 2013. “Analysis of daily, monthly,
782 and annual burned area of the fourth-generation global fire emissions database
783 (GFED4).” *Journal of Geophysical Research* 118(1): 317-328.
784 doi:10.1002/jgrg.20042.
- 785 Giglio, L. 2015. “MODIS Collection 6 Active Fire Product User’s Guide Revision A.”
786 [https://cdn.earthdata.nasa.gov/conduit/upload/3865/MODIS_C6_Fire_User_Gui](https://cdn.earthdata.nasa.gov/conduit/upload/3865/MODIS_C6_Fire_User_Guide_A.pdf)
787 [de_A.pdf](https://cdn.earthdata.nasa.gov/conduit/upload/3865/MODIS_C6_Fire_User_Guide_A.pdf)
- 788 Giglio, L., L. Boschetti, D. Roy, A. A. Hoffmann, and M. Humber. 2016. “Collection 6
789 MODIS Burned Area Product User’s Guide Version 1.0.” [http://modis-](http://modis-fire.umd.edu/files/MODIS_C6_BA_User_Guide_1.0.pdf)
790 [fire.umd.edu/files/MODIS_C6_BA_User_Guide_1.0.pdf](http://modis-fire.umd.edu/files/MODIS_C6_BA_User_Guide_1.0.pdf)
- 791 Gorelick, N., M. Hancher, M. Dixon, S. Ilyushchenko, D. Thau, and R. Moore. 2017.
792 “Google Earth Engine: Planetary-scale geospatial analysis for
793 everyone.” *Remote Sensing of Environment*. 202: 18-27.
794 doi:10.1016/j.rse.2017.06.031.
- 795 Government of Punjab. 2007. *State of environment*. Chandigarh: Punjab State Council
796 of Science and Technology.
- 797 Gupta, R. 2012. *Causes of Emissions from Agricultural Residue Burning in North-West*
798 *India: Evaluation of a Technology Policy Response*. SANDEE Working Paper
799 No. 66–12.
- 800 Jain, N., A. Bhatia, and H. Pathak. 2014. “Emission of Air Pollutants from Crop
801 Residue Burning in India.” *Aerosol and Air Quality Research*. 14: 422-430.
802 doi:10.4209/aaqr.2013.01.0031.
- 803 Kaskaoutis, D. G., S. Kumar, D. Sharma, R. P. Singh, S. K. Kharol, M. Sharma, A. K.
804 Singh, S. Singh, A. Singh, and D. Singh. 2014. “Effects of crop residue burning
805 on aerosol properties, plume characteristics, and long-range transport over

- 806 northern India.” *Journal of Geophysical Research*. 119: 5424–5444, doi:
807 10.1002/2013JD021357.
- 808 Key, C. H. and N. C. Benson. 2006. “Landscape assessment (LA): Sampling and
809 analysis methods. In D. C. Lutes, R. E. Keane, J. F. Caratti, C. H. Key, N. C.
810 Benson, S. Sutherland, and L. J. Gangi (Eds.)” *FIREMON: Fire effects*
811 *monitoring and inventory system*. General Technical Report RMRS-GTR-164-
812 CD (pp. LA1–LA51). Rocky Mountain Research Station, Fort Collins, CO:
813 United States Department of Agriculture, Forest Service.
814 http://www.fs.fed.us/rm/pubs/rmrs_gtr164.pdf.
- 815 Kumar, P., S. Kumar, and L. Joshi. 2015. *Socioeconomic and Environmental*
816 *Implications of Agricultural Residue Burning: A Case Study of Punjab, India*.
- 817 Landis, J. R. and G. G. Kock. 1977. “The Measurement of Observer Agreement for
818 Categorical Data.” *Biometrics* 33(1): 159-174. doi:10.2307/2529310.
- 819 Levy, R. C., S. Mattoo, L. A. Munchak, L. A. Remer, A. M. Sayer, F. Patadia, and N.
820 C. Hsu. 2013. “The Collection 6 MODIS aerosol products over land and ocean.”
821 *Atmospheric Measurement Techniques* 6(11): 2989-3034. doi:10.5194/amt-6-
822 2989-2013.
- 823 Lewis, S. A., A. T. Hudak, R. D. Ottmar, P. R. Robichaud, L. B. Lentile, S. M. Hood, J.
824 B. Cronan, and P. Morgan. 2011. Using hyperspectral imagery to estimate forest
825 floor consumption from wildfire in boreal forests of Alaska, USA. *International*
826 *Journal of Wildland Fire*. 20: 255-271. doi:10.1071/WF09081.
- 827 Liu, T., M. E. Marlier, R. S. DeFries, D. M. Westervelt, K. R. Xia, A. M. Fiore, L. J.
828 Mickley, D. H. Cusworth, and G. Milly. 2018. “Seasonal impact of regional
829 outdoor biomass burning on air pollution in three Indian cities: Delhi,
830 Bengaluru, and Pune.” *Atmospheric Environment*. 172: 83-92.
831 doi:10.1016/j.atmosenv.2017.10.024.
- 832 Loboda, T., K. J. O’Neal, and I. Csiszar. 2007. “Regionally adaptable dNBR-based
833 algorithm for burned area mapping from MODIS data.” *Remote Sensing of*
834 *Environment* 109(4): 429-442. doi:10.1016/j.rse.2007.01.017.
- 835 Mahajan, G., V. Kumar, and B. S. Chauhan. 2017. “Rice Production in India.” In: B.
836 Chauhan, K. Jabran, G. Mahajan G. (eds). *Rice Production Worldwide*.
837 Springer, Cham. doi:10.1007/978-3-319-47516-5_3.
- 838 McCarty, J. L., S. Korontzi, and S. Trigg. 2008. “A hybrid remote sensing approach to
839 quantifying crop residue burning in the United States.” *Applied Engineering in*
840 *Agriculture* 24(4): 515-527. doi:10.13031/2013.25137.
- 841 McCarty, J. L., S. Korontzi, C. O. Justice, and T. Loboda. 2009. “The spatial and
842 temporal distribution of crop residue burning in the contiguous United States.”
843 *Science of The Total Environment* 407(15): 5701-5712.
844 doi:10.1016/j.scitotenv.2009.07.009.
- 845 Mehta, C. R., N. S. Chandel, T. Senthilkumar, and K. K. Singh. 2014. “Trends of
846 Agricultural Mechanisation in India.” *ESCAP/CSAM Policy Brief*, Issue No. 2.
847 <http://www.un-csam.org/publication/PB201402.pdf>.
- 848 Misri, B. K. 1999. *Country Pasture/Forage Resources Profiles, India*.
849 <http://www.fao.org/ag/AGP/AGPC/doc/Counprof/India.htm>.

- 850 Mu, M., J. T. Randerson, G. R. van der Werf, L. Giglio, P. Kasibhatla, D. Morton, G.
851 J. Collatz, R. S. DeFries, E. J. Hyer, E. M. Prins, D. W. T. Griffith, D.
852 Wunch, G. C. Toon, V. Sherlock, and P. O. Wennberg. 2011. "Daily and 3-
853 hourly variability in global fire emissions and consequences for atmospheric
854 model predictions of carbon monoxide." *Journal of Geophysical Research:*
855 *Atmospheres*. 116: D24303. doi:10.1029/2011JD016245.
- 856 Munchak, L. A., R. C. Levy, S. Mattoo, L. A. Remer, B. N. Holben, J. S. Schafer, C. A.
857 Hostetler, and R. A. Ferrare. 2013. "MODIS 3 km aerosol product: applications
858 over land in an urban/suburban region." *Atmospheric Measurement Techniques*
859 6(7): 1747-1759. doi:10.5194/amt-6-1747-2013.
- 860 Oliva, P. and W. Schroeder. 2015. "Assessment of VIIRS 375 m active fire detection
861 product for direct burned area mapping." *Remote Sensing of Environment* 160:
862 144-155. doi:10.1016/j.rse.2015.01.010.
- 863 Picotte, J. J. and K. M. Robertson. 2010. "Accuracy of remote sensing wildland fire-
864 burned area in southeastern U.S. Coastal Plain habitats." In K. M. Robertson, K.
865 E. M. Galley, and R. E. Masters (eds.). *Proceedings of the 24th Tall Timbers*
866 *Fire Ecology Conference: The Future of Prescribed Fire: Public Awareness,*
867 *Health, and Safety. Tall Timbers Research Station, Tallahassee, Florida, USA.*
- 868 Pleniou, M. and N. Koutsias. 2013. "Sensitivity of spectral reflectance values to
869 different burn and vegetation ratios: A multi-scale approach applied in a fire
870 affected area." *ISPRS Journal of Photogrammetry and Remote Sensing* 79: 199-
871 210. doi:10.1016/j.isprsjprs.2013.02.016.
- 872 Punia, M., V. P. Nautiyal, and Y. Kant. 2008. "Identifying biomass burned patches of
873 agriculture residue using satellite remote sensing data." *Current Science* 94(9):
874 1185-1190.
- 875 Punjab Remote Sensing Centre (PRSC), Ludhiana. 2015. *Monitoring Residue Burning*
876 *through Satellite Remote Sensing.* Punjab Pollution Control Board, Patiala.
- 877 Randerson, J. T., Y. Chen, G. R. van der Werf, B. M. Rodgers, and D. C. Morton. 2012.
878 "Global burned area and biomass burning emissions from small fires." *Journal*
879 *of Geophysical Research* 117(4): G04012. doi:10.1029/2012JG002128.
- 880 Rogan, J. and S. R. Yool. 2001. "Mapping fire-induced vegetation depletion in the
881 Peloncillo Mountains: Arizona and New Mexico." *International Journal of*
882 *Remote Sensing* 22(16): 3101-3121. doi:10.1080/01431160152558279.
- 883 Roy, D. P. 1999. "Multi-temporal active-fire based burn scar detection algorithm."
884 *International Journal of Remote Sensing* 20(5): 1031-1038.
885 doi:10.1080/014311699213073.
- 886 Roy, D. P., Y. Jin, P. E. Lewis, and C. O. Justice. 2005. "Prototyping a global algorithm
887 for systematic fire-affected area mapping using MODIS time series data."
888 *Remote Sensing of Environment* 97(2): 137-162. doi:10.1016/j.rse.2005.04.007.
- 889 Sayer, A. M., N. C. Hsu, C. Bettenhausen, and M-J. Jeong. 2013. "Validation and
890 uncertainty estimates for MODIS Collection 6 "Deep Blue" aerosol data."
891 *Journal of Geophysical Research: Atmospheres* 118(14): 7864-7872.
892 doi:10.1002/jgrd.50600.
- 893 Sharma, A. R., S. K. Kharol, K. V. S. Badarinath, and D. Singh. 2010. "Impact of
894 agriculture crop residue burning on atmospheric aerosol loading – a study over

- 895 Punjab State, India.” *Annales Geophysicae* 28(2): 367-379.
- 896 Sidhu, B. S., and V. Beri. 2005. “Experience with managing rice residues in intensive
897 rice-wheat cropping system in Punjab.” In I. P. Abrol, R. K. Gupta, and R. K.
898 Malik (Eds.), *Conservation agriculture: Status and prospects* 55-63. New Delhi:
899 Centre for Advancement of Sustainable Agriculture, National Agriculture
900 Science Centre.
- 901 Singh, G., Y. Kant, and V. K. Dadhwal. 2009. “Remote sensing of crop residue burning
902 in Punjab (India): a study on burned area estimation using multi-sensor
903 approach.” *Geocarto International* 24(4): 273-292.
904 doi:10.1080/10106040802556181.
- 905 Singh, K. 2009. “Act to Save Groundwater in Punjab: Its Impact on Water Table,
906 Electricity Subsidy and Environment.” *Agricultural Economics Research
907 Review* 22: 365-386.
- 908 Singh, M. K., R. Gautam, and P. Venkatachalam 2017. “Bayesian Merging of MISR
909 and MODIS Aerosol Optical Depth Products Using Error Distributions From
910 AERONET.” *IEEE Journal of Selected Topics in Applied Earth Observations
911 and Remote Sensing* PP(99): 1-15. doi:10.1109/JSTARS.2017.2734331.
- 912 Singh, R. P., H. S. Dhaliwal, H. S. Sidhu, Y. S. Manpreet-Singh, and J. Blackwell.
913 2008. “Economic assessment of the Happy Seeder for rice-wheat systems in
914 Punjab, India.” Conference Paper, AARES 52nd Annual conference, Canberra.
915 Australia: ACT.
- 916 Strauss, M. 2017. “Planet Earth to get a daily selfie.” *Science* 355(6327): 782-783.
917 doi:10.1126/science.355.6327.782.
- 918 Thumaty, K. C., S. R. Rodda, J. Singhal, R. Gopalakrishnan, C. S. Jha, G. D. Parsi, and
919 V. K. Dadhwal. 2015. “Spatio-temporal characterisation of agriculture residue
920 burning in Punjab and Haryana, India, using MODIS and Suomi NPP VIIRS
921 data.” *Current Science* 109(10): 1850-1855. doi:10.18520/v109/i10/1850-1855.
- 922 Vadrevu, K. P., E. Ellicott, and K. Badarinath. 2011. “MODIS derived fire
923 characteristics and aerosol optical depth variations during the agricultural
924 residue burning season, north India.” *Environmental Pollution* 159(6): 1560-
925 1569. doi:10.1016/j.envpol.2011.03.001.
- 926 van der Werf, G. R., J. T. Randerson, L. Giglio, G. J. Collatz, M. Mu, P. S. Kasibhatia,
927 D. C. Morton, R. S. DeFries, Y. Jin, and T. T. van Leeuwen. 2010. “Global fire
928 emissions and the contribution of deforestation, savanna, forest, agricultural, and
929 peat fires (1997-2009).” *Atmospheric Chemistry and Physics* 10(23): 11707-
930 11735. doi:10.5194/acp-10-11707-2010.
- 931 van der Werf, G. R., J. T. Randerson, L. Giglio, T. T. van Leeuwen, Y. Chen, B. M.
932 Rogers, M. Mu, M. J. E. van Marle, D. C. Morton, G. J. Collatz, R. J. Yokelson,
933 P. S. Kasibhatla. 2017. “Global fire estimates during 1997-2016.” *Earth System
934 Science Data* 9:687-720. doi:10.5194/essd-2016-62.
- 935 Vermote, E. F. and S. Kotchenova. 2008. “Atmospheric correction for the monitoring of
936 land surfaces.” *Journal of Geophys Research* 113: D23S90.
937 doi:10.1029/2007JD009662
- 938 United Nations, Department of Economic and Social Affairs, Population Division.
939 2015. *World Population Prospects: The 2015 Revision, Key Findings and*

- 940 *Advance Tables Working Paper No. ESA/P/WP.241.*
- 941 Wang, Q., G. A. Blackburn, A. O. Onojeghuo, J. Dash, L. Zhou, Y. Zhang, and P. M.
942 Atkinson. 2017. "Fusion of Landsat 8 OLI and Sentinel-2 MSI Data." *IEEE*
943 *Transactions on Geoscience and Remote Sensing* 55(7): 3885-3899. doi:
944 10.1109/TGRS.2017.2683444.
- 945 Xiang, H.-B. 2013. "Algorithms for Moderate Resolution Imaging Spectroradiometer
946 cloud-free image compositing." *Journal of Applied Remote Sensing* 7: 073486.
947 doi: 10.1117/1.JRS.7.073486.
- 948 Yadav, M., M. P. Sharma, R. Prawasi, R. Khichi, P. Kumar, V. P. Mandal, A. Salim,
949 and R. S. Hooda. 2014a. "Estimation of Wheat/Rice Residue Burning Areas in
950 Major Districts of Haryana, India, Using Remote Sensing Data." *Journal of the*
951 *Indian Society of Remote Sensing*. 42(2): 343-352. doi:10.1007/s12524-013-
952 0330-z.
- 953 Yadav, M., R. Prawasi, S. Jangra, P. Rana, K. Kumari, S. Lal, K. Jakhar, S. Sharma, and
954 R. S. Hooda. 2014b. "Monitoring seasonal progress of rice stubble burning in
955 districts of Haryana, India, using multirate AwiFS data." *The International*
956 *Archives of the Photogrammetry, Remote Sensing and Spatial Information*
957 *Sciences*. 40(8): 1003-1009. doi:10.5194/isprsarchives-XL-8-1003-2014.
- 958 Zhu, C., H. Kobayashi, Y. Kanaya, and M. Saito. 2017. Size-dependent validation of
959 MODIS MCD64A1 burned area over six vegetation types in boreal Eurasia:
960 Large underestimation in croplands. *Scientific Reports*. 7: 4181.
961 doi:10.1038/s41598-017-03739-0.



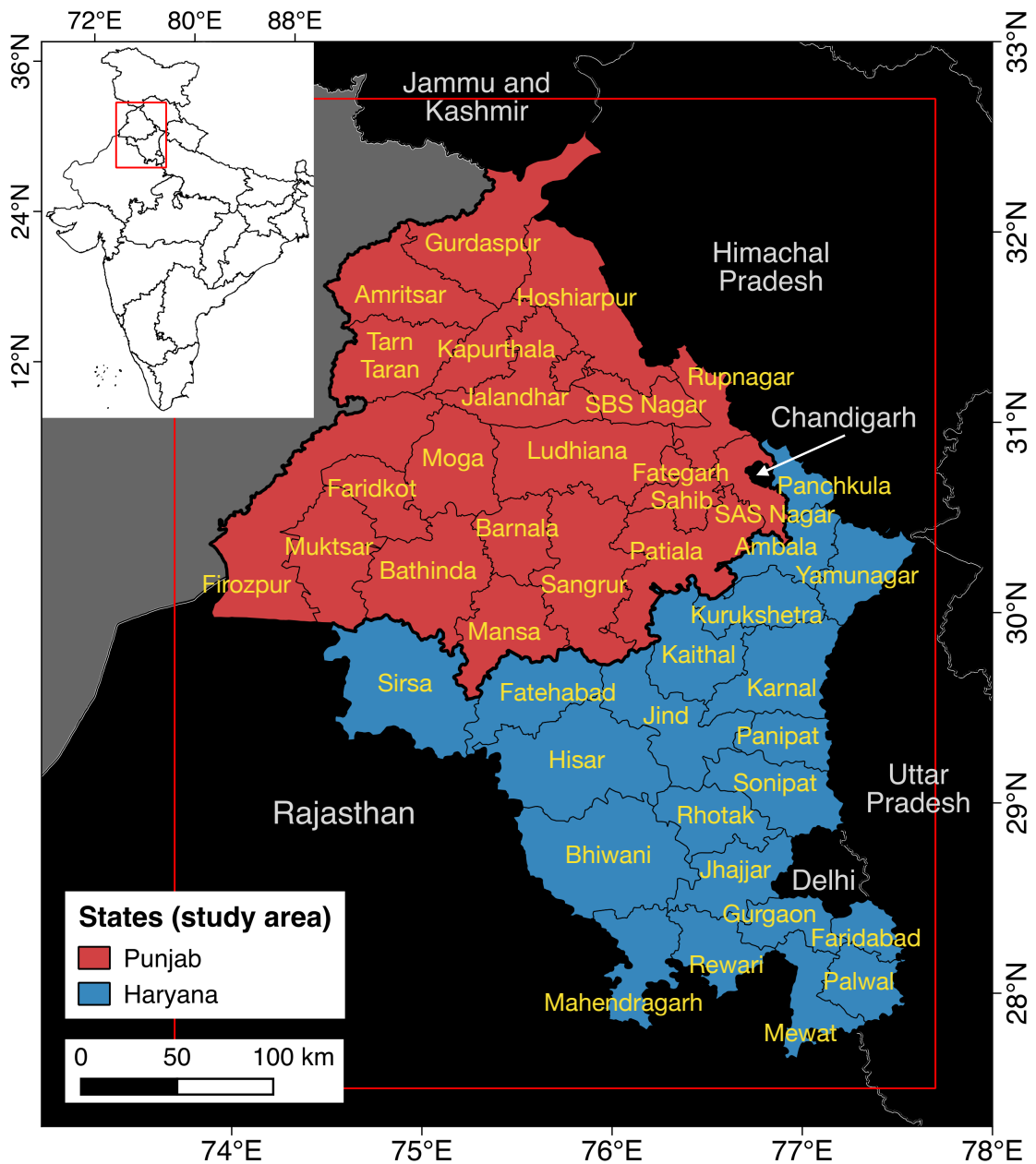
962

963

964

965

Figure 1. Example of thick haze over northern India during the post-monsoon burning season: True colour MODIS/Aqua on November 6, 2016 (NASA Worldview). The study area is bounded by a red box.



966

967

968

969

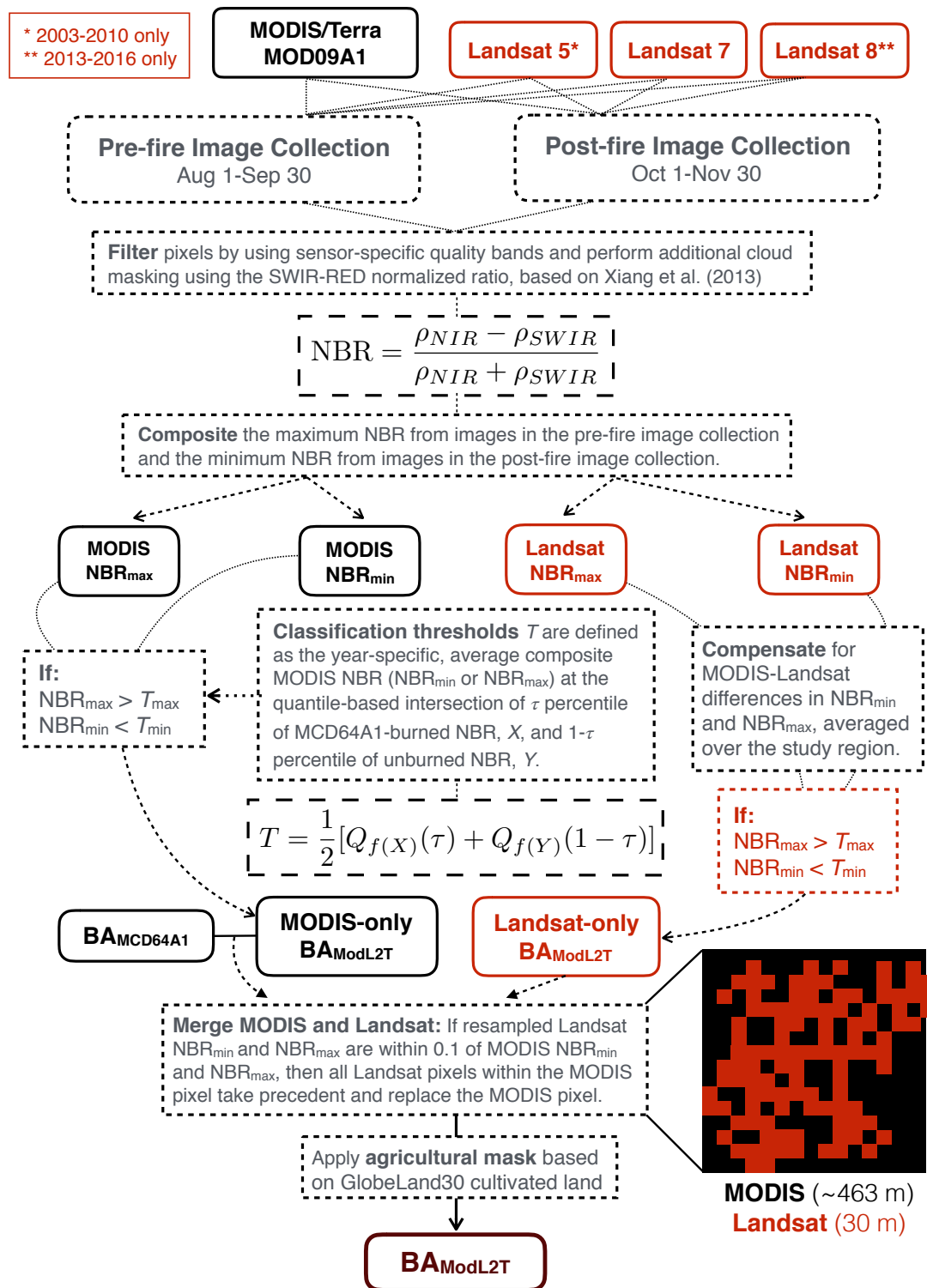
970

Figure 2. District-level maps of the study area: Punjab (red) and Haryana (blue), two agricultural states in northwestern India. District administrative borders are from the 2011 Indian census. *Inset:* The red box shows the location of the study area in a zoomed-out view of states in India, excluding the seven sister states.

971 **Table 1.** Satellite-derived products used in this study.

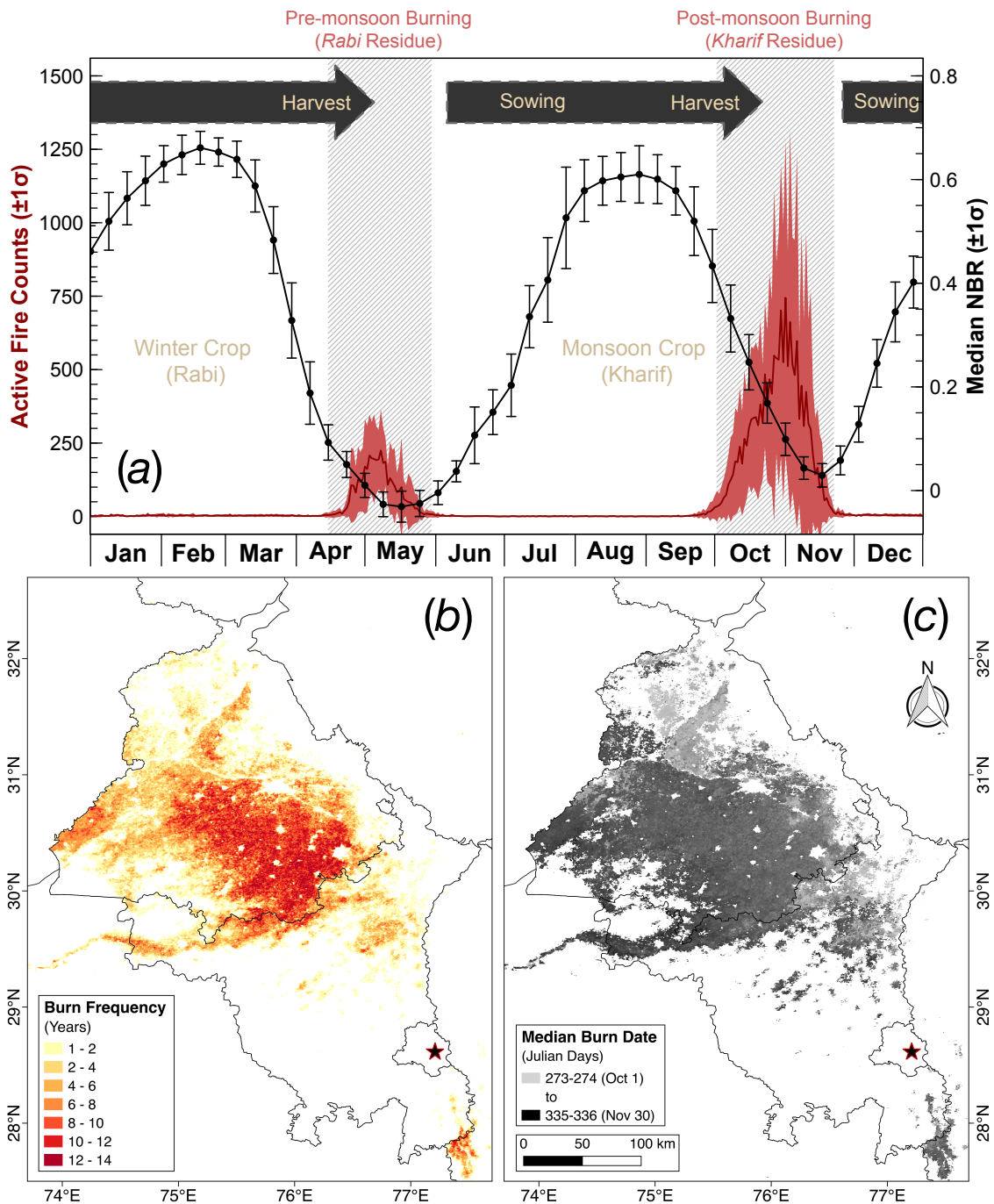
Satellite/ Product	Sensor	Description	Product Code	Resolution		Availability
				Spatial	Temporal	
Landsat 5	TM					1984-2013
Landsat 7	ETM+					from 1999
Landsat 8	OLI/ TIRS	Surface Reflectance	SR	30 m	once every 16 days	from 2013
			MOD09A1	500 m	8-day composite	from 2000
		Active Fires	MCD14ML	1 km	daily	
Terra/ Aqua	MODIS	Burned Area	MCD64A1	500 m	monthly	<i>Terra:</i> from 2000
		AOD	MOD04/ MYD04	10 km	daily	<i>Aqua:</i> from 2002
			MOD04_3K/ MYD04_3K	3 km		
Global Fire Emissions Database		Emissions	GFEDv4s	0.25°	monthly 3-hourly	from 1997 from 2003
Suomi NPP	VIIRS	Active Fires	VNP14IMG ML	375 m	daily	from 2012
GlobeLand30		Land Cover	—	30 m		2000, 2010

972



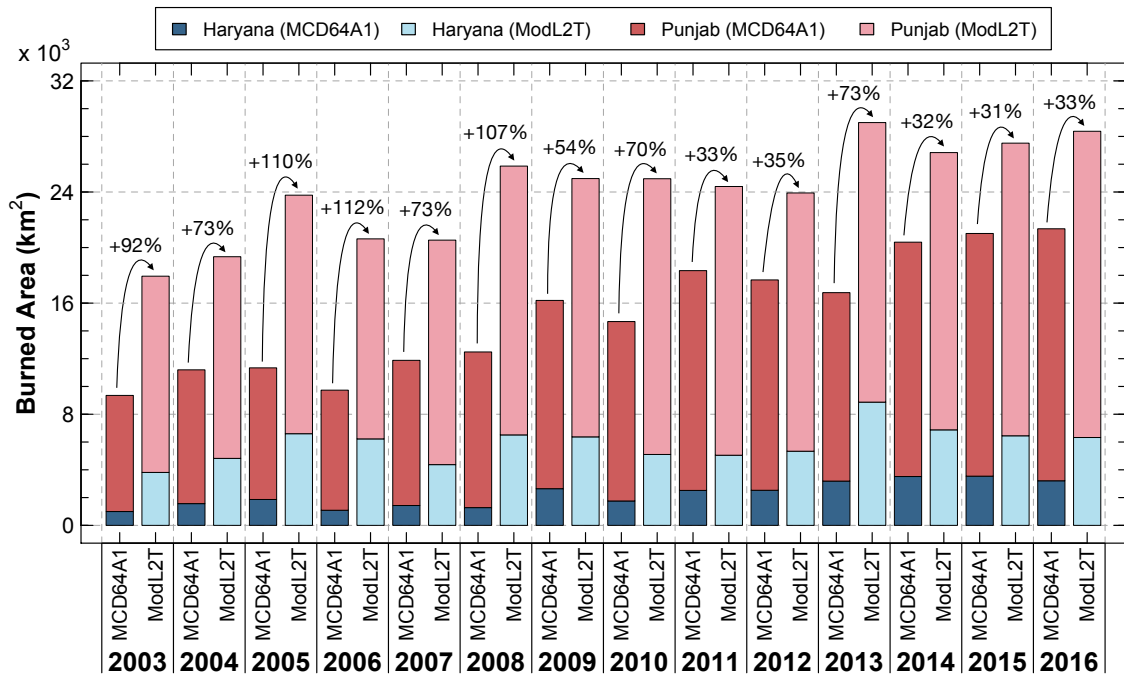
973

974 **Figure 3. Workflow of the ModL2T algorithm:** estimation of post-monsoon
 975 (October-November) agricultural burned area. The final ModL2T burned area is 30 m x
 976 30 m in spatial resolution. The inset schematic shows Landsat burned pixels (red)
 977 overlain on a MODIS burned pixel (black); if the MODIS-Landsat merging criteria are
 978 met, then the ~238 Landsat pixels replace the MODIS pixel.



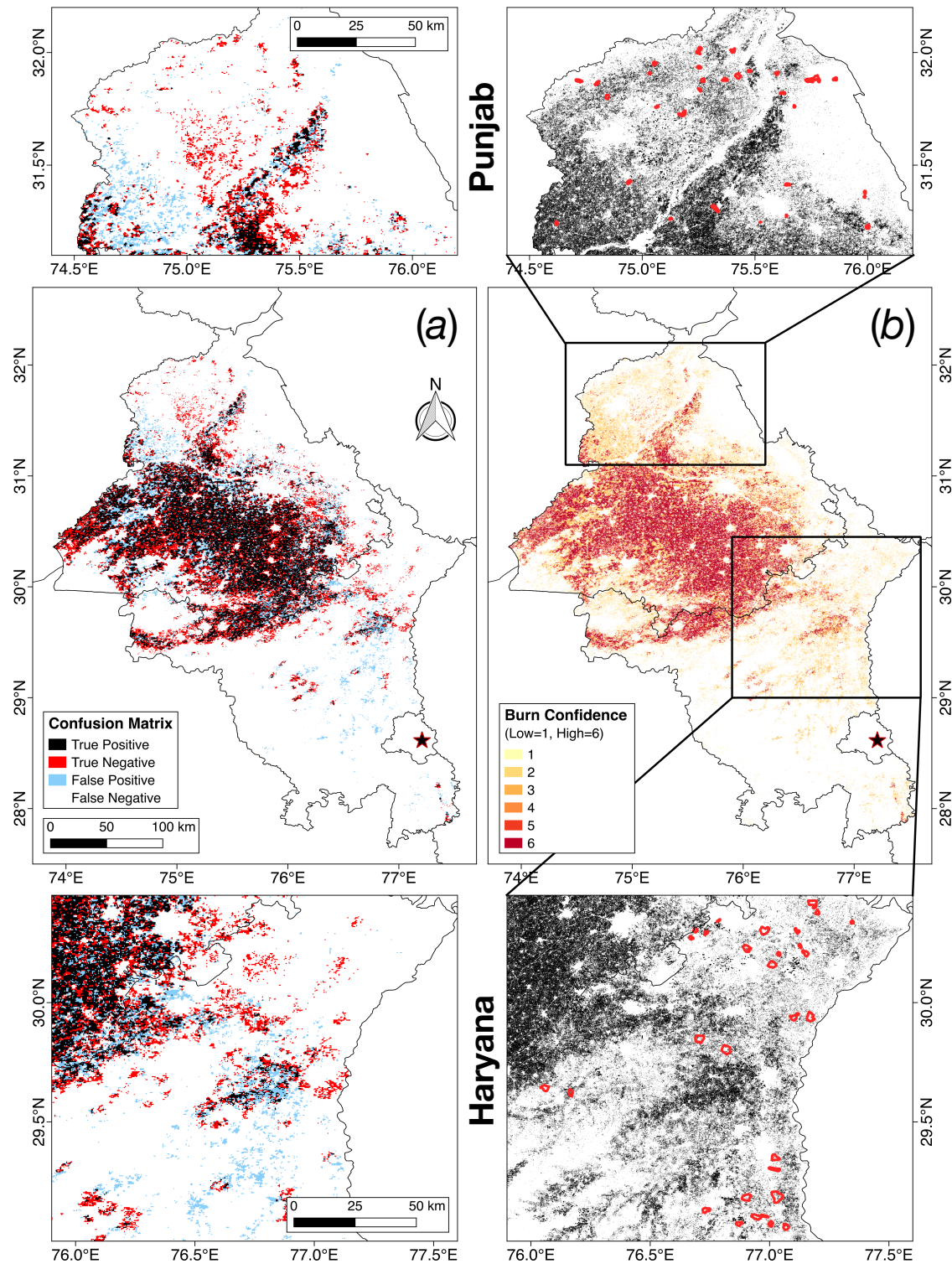
979

980 **Figure 4. Spatio-temporal overview of agricultural burning in northwestern India:**
 981 (a) The double crop-fire cycle, following Vadrevu et al. (2011), using daily MODIS fire
 982 counts and 8-day composite median NBR, with $\pm 1\sigma$ envelopes, in Punjab and Haryana,
 983 2003-2016. Post-monsoon (October-November) (b) burn frequency and (c) median burn
 984 date based on $BA_{MCD64A1}$. The colour bar is discrete in (b) and continuous in (c). The
 985 star denotes the location of New Delhi.



986

987 **Figure 5. Total agricultural burned area: $BA_{MCD64A1}$ and BA_{ModL2T} in Punjab (red**
 988 **shades) and Haryana (blue shades) during post-monsoon (October-November), 2003-**
 989 **2016. The ModL2T algorithm estimates $66 \pm 31\%$ higher post-monsoon burned area in**
 990 **Punjab and Haryana than MCD64A1.**



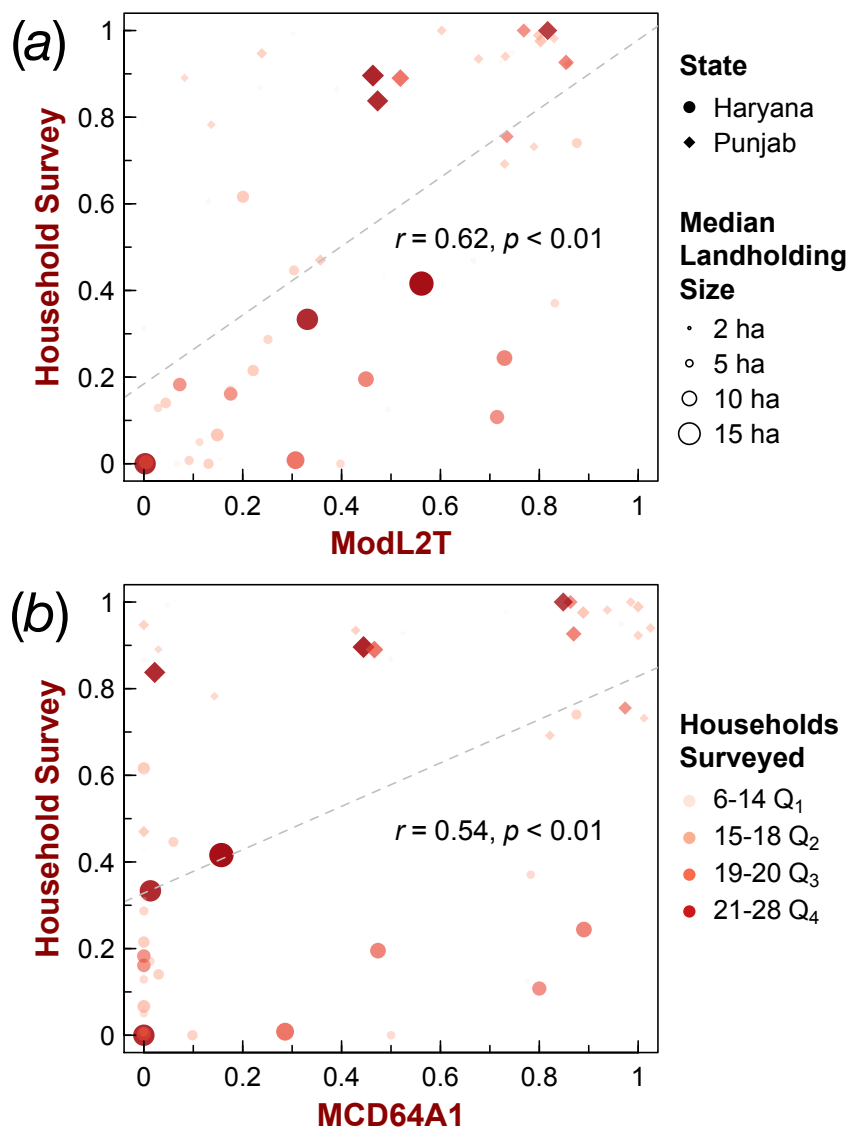
991

992 **Figure 6. ModL2T burned area classification:** (a) Agreement between $BA_{MCD64A1}$
 993 and MODIS-only BA_{ModL2T} and (b) classification confidence (Low = 1, High = 6) for
 994 BA_{ModL2T} in Haryana and Punjab, post-monsoon (October-November) in 2016. The
 995 zoomed-in images show BA_{ModL2T} (black) and the locations of the villages (red
 996 polygons) in Punjab (top row) and Haryana (bottom row) surveyed in 2016 for
 997 validation. The star denotes the location of New Delhi.

998 **Table 2.** Geographical accuracy assessment of BA_{MCD64A1} (reference) and MODIS-only
 999 BA_{ModL2T}, in Punjab and Haryana, post-monsoon (October-November) in 2016 ($\kappa =$
 1000 0.53, moderate agreement)

MODIS-only BA _{ModL2T}	MCD64A1		Producer's Accuracy
	Burned	Unburned	
Burned	67640	49483	0.58
Unburned	31497	362042	0.92
User's Accuracy	0.68	0.88	0.84

1002



1003

1004

1005

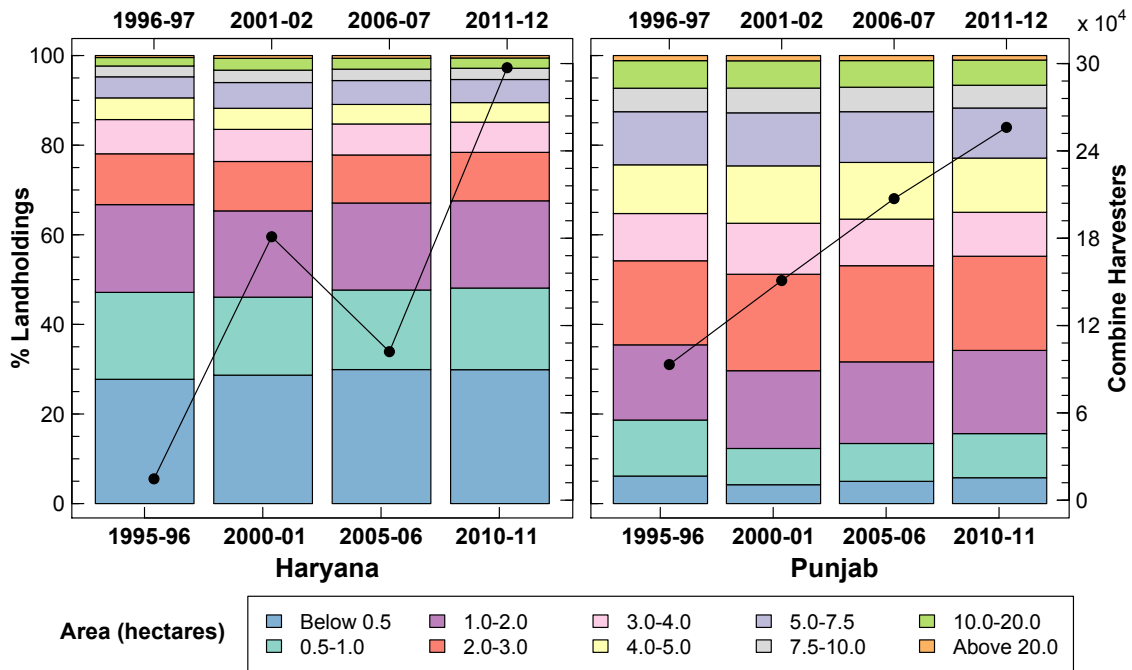
1006

1007

1008

1009

Figure 7. Validation of satellite-derived burned area using household surveys: comparison of % burning activity, normalised by landholding size and % burned area from (a) ModL2T and (b) MCD64A1 in 30 Punjab (diamonds) and 32 Haryana (circles) villages during post-monsoon (October-November) in 2016. The size of the markers denotes the median landholding size, and the colour denotes the quartile of the number of households surveyed.



1010

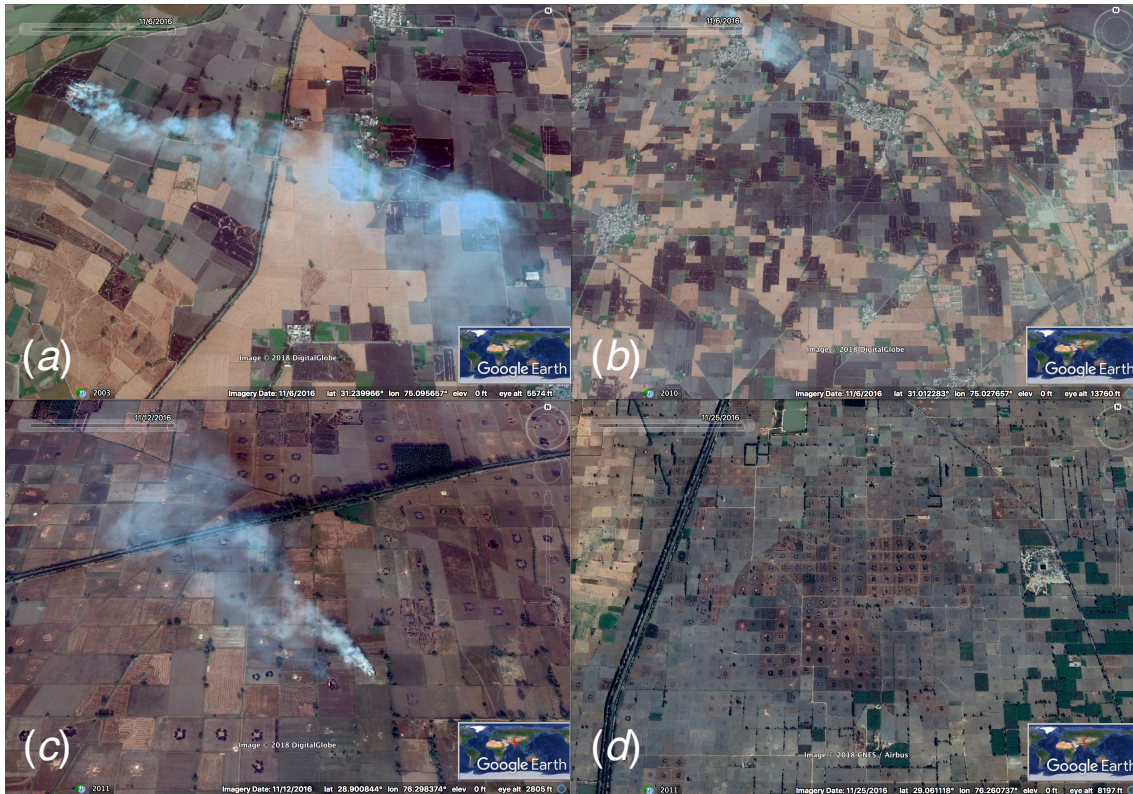
1011

1012

1013

1014

Figure 8. Trends in landholdings by size and in use of combine harvesters in Punjab and Haryana: Data from the Agricultural Census are in quinquennial intervals from 1995-96 to 2010-11 (landholdings) and the Input Survey, from 1996-97 to 2011-12 (combine harvesters).



1015

1016

1017

1018

1019

Figure 9. Two crop residue burning practices: Fine-resolution Google Earth DigitalGlobe and CNES/Airbus historical imagery of smoke and burn scars from crop residue burning in (a-b) central-northern Punjab (whole field) and (c-d) central Haryana (primarily partial field) in November 2016.